# POLITECNICO DI TORINO

Corso di Laurea Magistrale

in **Ingegneria Energetica e Nucleare**

Tesi di Laurea Magistrale

# Tri-generation plant based on SOFC for dynamic hydrogen production


Relatori

Prof. Massimo Santarelli

Prof. Jack Brouwer

Dr. Marta Gandiglio

Candidato:

Vito Pinto


Ottobre 2019

# *Acknowledgments*

*The success of this work needs to be shared with my supervisors, professors Massimo Santarelli, Marta Gandiglio and Jack Brouwer because they gave me the opportunity to work on my thesis in a challenging and forefront environment at University of California, Irvine. This experience has been a growth in the academic but especially in the personal sphere.*

*Thanks to my family, because through their sacrifices they allowed me to follow my own path without ever hindering me.*

*Thanks to my office mates in UCI, Alireza, Laura, Yanchen for supporting me in difficult situations and for sharing with me my first goals. Special thanks to Luca, for being much more than a technical and moral support during the months abroad.*

*Thanks to all the classmates, friends, cousins, relatives and people that I met during this amazing journey because everyone has enriched my life.*

*Thanks to those who are not here but wished to be.*

# Contents

## Abstract

The tri-generation concept on High Temperature Fuel Cell (HTFC) is one of the most interesting solutions to convert efficiently a variety of fuels into electrical power, heat, and hydrogen on a distributed scale. The exceptional performance of the Solid Oxide Fuel Cell (SOFC) can be exploited even more with a tri-generation operation when biogas from anaerobic digester is supplied. The first perk consists in the use of a valuable source recovered from waste product, in a device that emits almost zero pollutants compared to traditional engines. Moreover, running the SOFC with a lower fuel utilization factor, the performance of the whole system improves thanks to the synergistic effect of three simultaneous phenomena: increased efficiency because of higher Nernst potential; less cooling load required by the fuel cell because the internal Steam Methane Reforming (SMR) that occurs inside the anode channel, it is an endothermic reaction; production of a third useful product, hydrogen, with the possibility of controlling its production on-demand. This study represents a sort of link between DEMOSOFC, one of the most important European projects regarding the installation of SOFC modules utilizing biogas as fuel in a Waste Water Treatment Plant (WWTP) located in Collegno (TO) in collaboration with Politecnico di Torino, and the first example in the world of a of tri-generation plant based on Molten Carbonate Fuel Cell (MCFC) installed in Orange County Sanitation District (OCSD) in collaboration with University of California, Irvine (UCI). The aim of this study was to understand the steady state and dynamic behavior of SOFC modules in a tri-generation plant configuration, explaining the differences with a normal co-generation mode. The nominal size of the fuel cell chosen for the work is the same size of one module installed in the real DEMOSOFC plant (58 kW). Several variables affect the outputs of the fuel cell and a sensitivity analysis upon some of them allowed to highlight a precise working condition of the device, near its thermoneutral condition, where the exothermicity of the SOFC becomes very small. In order to limit the temperature drop at the very beginning of the cell due to the SMR and the instability found in terms of current density when pure biogas (with the proper Steam-to-Carbon ratio) is supplied to the SOFC, four reformates cases have been evaluated and the one that showed

the best features has been selected for the following simulations. Once the steady state results of the stack have been illustrated, the steady state design conditions of the plant with a fuel cell utilization factor of 60% are presented and justified as well, showing a production of about 1.06 kg/h of hydrogen for each module downstream the Hydrogen Separation Unit (HSU). The second focus of the work consisted in studying the dynamic of the system and how the SOFC can be controlled (through a PI controller) in order to limit thermal stresses and temperature fluctuations of the Positive-Electrolyte-Negative layer (PEN) but regulating the production of the three products. Two main logics of dynamics have been evaluated, regarding a change in power load of the SOFC and the fuel utilization factor. The results showed a good response of the fuel cell, even considering the different timescales between the thermal and electrochemical phenomena. The Supplemental Input Method has been used to calculate the efficiencies of the system for each product of the polygeneration plant, resulting in efficiency of 74.5% for the hydrogen production purpose. Moreover, a comparison with the state-of-the-art technologies has been provided in terms of Primary Energy Savings (PES) where 16% of the total energy input could be saved if the tri-generation plant were used. A literature comparison especially with the MCFC previously mentioned showed that the SOFC performed better in terms of both electrical efficiency and hydrogen production. A descriptive chapter about the uses of the hydrogen and the possibility to build a distributed infrastructure with several installations in WWTPs concludes the study.

# List of figures

## List of tables

## List of acronyms

| | |
|---|---|
| AD | Anaerobic Digestion |
| BoP | Balance of the Plant |
| COD | Chemical Oxygen Demand |
| CV | Control Volume |
| DIR | Direct Internal Reforming |
| DoE | Department of Energy |
| FCB | Fuel Cell Bus |
| FCV | Fuel Cell Vehicle |
| FEM | Finite Element Method |
| GHG | Green House Gases |
| GUI | Graphic User Interface |
| HSU | Hydrogen Separation Unit |
| HTFC | High Temperature Fuel Cell |
| HX | Heat exchanger |
| IEA | International Energy Agency |
| LHV | Lower Heating Value |
| LSM | Lanthanium Strontium Manganite |
| MCFC | Molten Carbonate Fuel Cell |
| NG | Natural Gas |
| NIST | National Institute of Standards and Technology |
| OCSD | Orange County Sanitation District |
| ODE | Ordinary Differential Equation |
| OFMSW | Organic Fraction of Municipal Solid Waste |
| P2G | Power to Gas |

| | |
|---|---|
| PEM | Proton Exchange Membrane |
| PEN | Positive-Electrolyte-Negative |
| PES | Primary Energy Savings |
| PI | Proportional Integral (controller) |
| PSA | Pressure Swing Adsorption |
| S/C | Steam to Carbon ratio |
| SECA | Solid State Energy Conversion Alliance |
| SIM | Supplemental Input Method |
| SMR | Steam Reforming Methane |
| SOFC | Solid Oxide Fuel Cell |
| TPB | Triple Phase Boundary |
| WGS | Water Gas Shift |
| WWTP | WasteWater Treatment Plant |
| YSZ | Yttria-stabilized-Zirconia |

# 1. Introduction

In 2018 the $CO_2$ emissions grew 1.7% and they reached the historic maximum of 33.1 Gt per year. Although the rate of increase in the GHG is reducing thanks to energy efficiency measures and greater use of renewables, the economic growth does not allow a net reduction in the total amount of GHG and pollutants emission per year [1], [2]. Several policies have been adopted in the paste decades in order to contain the global warming phenomenon with the detachment from fossil fuels ([3], [4]). To accomplish those goals, it is necessary to invest in clean technologies for electricity generation, to employ alternative fuels in the transportation field, and using waste rationally through which it is possible to recover valuable products. One of the most important means already available is the use of the simplest chemical element, hydrogen.

## 1.1. Hydrogen is the way

The first consequence in the use of hydrogen as fuel is the lack of carbon in its structure which means no carbon dioxide production. Looking over the low environmental impact and its great energy density per mass thanks to its lightness, the hydrogen flexibility is another important benefit because it can be used for energy storage or mobility purposes. Several countries like Japan, Germany and California (USA) started investing heavily in hydrogen infrastructure and technologies, as confirmed by the first Olympic games in Tokyo where staff and athletes will be moving on board of FCVs and FCBs in 2020 ([5], [6]), the first hydrogen-powered train in the northern Germany ([7]), and the massive hydrogen refueling stations in California thanks to the developed FCVs market and government policy towards a 100% renewable and zero carbon energy by 2045 ([8], [9]). Besides the features already described, the hydrogen is the main alternative to fossil fuels in the transportation sector together with all-electric vehicles. Japan, South Korea, California and Germany are the countries in which the FCV market is increasing, mainly because of the investment in hydrogen fueling stations and government incentives. For example, in California the best-selling car is Toyota Mirai at the beginning of 2018, which counts more than 3,000 units. According to [10], the 113 kW of PEM fuel cell of the Mirai has the lowest consumption among the FCVs commercialized, able to travel 66 miles per kg of

$H_2$, accounting for a total range miles of 312 mi. The fuel cell system cost is reducing year by year (initially thanks to the government incentives) and it is going to approach the value of 40$/kW foreseen by DoE at 2020. Furthermore, the advantage with respect to the all-electric vehicles mentioned is that fuel cells do not use lithium and cobalt as the batteries do. Their reserves are limited, and their prices is increasing exponentially [11]. The latter consideration is also one of the reasons why the hydrogen can be seen as a better energy storage candidate than batteries, especially for large-scale and long duration storage, in addition to the higher energy density and the lack of the self-discharge phenomenon [12]. Moreover, hydrogen has a great potential because it is the starting point to build several fertilizers and chemicals, so its flexibility in uses and production opens several strategies that can be evaluated and pursued. However, hydrogen is not spontaneously available, and its production has a key role in the determination of its final cost which affect his spread and use. According to DoE Hydrogen and Fuel Cells program, hydrogen threshold cost is around $2–4/kg, to be competitive with advanced hybrid vehicles [13]. There are different ways of producing hydrogen: thermochemically, biochemically, electrochemically or through emerging techniques such as chemical looping and photocatalytic process, but the state of the art production relies largely on fossil fuel energy input (e.g. steam methane reforming) ([14]–[16]). The electrochemical path, through electrolysis, is another mature market product that is getting and increasingly larger part of the market, in particular when the excess renewable energy is used in the power to gas (P2G) concept [17]. Every year the installed capacity of photovoltaic and wind farms increases, facing the big challenge of the grid management, but instead of curtailing the excess electricity from renewable in certain periods of the year (and of the day) the electrolysis allows the production of hydrogen that can be stored and used later. The following storage and transportation of the hydrogen present other different solutions which should be evaluated for each different final use of the hydrogen: for example, the injection into the existing NG pipelines is a low cost and a ready to use mean to develop the hydrogen infrastructure and availability across each country, both for a storage perspective and use in power plants [12]. The first demonstration in the United States of the power-to-gas hydrogen pipeline injection has been implemented by University of California,

Irvine in the campus network and the blended hydrogen in the natural gas pipeline is used on the cogeneration plant of the campus itself [18], [19]. In Europe, Germany is the country that invested the most on this technology in the past years carrying out several projects exploiting the excess from wind farms. In Italy, SNAM® launched its experiment of hydrogen injection at 5% in the natural gas pipeline at regional level [20]. This concept is often related to the more general discussion between the concentrated or distributed strategy for hydrogen production. Brouwer et al. [21] showed that the best choice in terms of supply chain efficiency corresponds to the distributed hydrogen production with HTFC working at low utilization factor, if transportation and storage is considered in the analysis followed by centralized SMR with compressed hydrogen distribution.

## 1.2. High Temperature Fuel Cell - SOFC

High temperature fuel cells present several perks with respect to other devices for cogeneration purpose (i.e. power and heat) because the high temperature (1) lead to high-quality heat downstream to be used for cogeneration purpose, (2) reduces the ohmic and activation losses of the cell and (3) it allows the cell to work on hydrocarbon fuel supply (i.e. NG, biogas, syngas,..) because the Direct Internal Reforming inside the anode compartment is easily practicable thanks to the faster kinetics even not using precious catalysts like in PEM fuel cells ([22], [23]). The state of the art for Solid Oxide Fuel Cell presents outstanding performance among the fuel cell types and they have been studying since several years in different contexts ([24]–[27]). Exploiting the capability of SOFC to process hydrocarbon fuels like biogas or NG, two main reactions occur in the anode channels:

SMR: $$CH_4 + H_2O \rightleftharpoons 3H_2 + CO \qquad \Delta H^0_{298} = 206\ kJ/mol \quad (1)$$

WGS: $$CO + H_2O \rightleftharpoons H_2 + CO_2 \qquad \Delta H^0_{298} = -41\ kJ/mol \quad (2)$$

The SMR is strongly endothermic whereas the WGS is slightly exothermic, so a certain amount of heat should be supplied to make the reactions happen before the delivered hydrogen could react electrochemically with the oxygen ions in the PEN layer [28] (Figure 1):

Anode $$H_2 + O^{2-} \rightarrow H_2O + 2e^- \quad (3)$$

Cathode $$\frac{1}{2}O_2 + 2e^- \rightarrow O^{2-} \quad (4)$$

Total $$H_2 + \frac{1}{2}O_2 \rightarrow H_2O \quad (5)$$

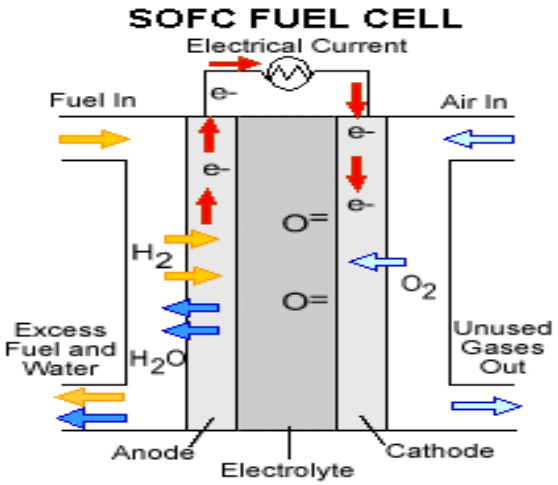


*Figure 1. SOFC electrochemical reactions.*

There are three possible structure of the SOFC, related to the thickest layer: cathode, electrolyte or anode supported. The three typologies differ both from the mechanical behavior and electrical performance. Historically, companies preferred to use cathode and electrolyte supported cell, but the new trend is moving on the anode supported which are the best in terms of performance since the diffusivity of the hydrogen molecules is higher than the oxygen ones (if it was cathode supported) and the main drop in voltage as ohmic loss occurs in the electrolyte layer which is thinner in the anode supported case. The state-of-the-art materials used in the commercial cells are a thin 8 mol% yttria-stabilized zirconia (YSZ) electrolyte, supported on a conventional porous Ni/YSZ anode electrode whereas the cathode electrode is constituted by a composite structure of metallic perovskite Sr-doped LaMnO3 (LSM) and oxide-ion conductive electrolyte YSZ [29].

## 1.3. Biogas as product from waste

The possibility of internal reforming inside the fuel cell opens the scenario of SOFC fed by biogas ([23], [25], [30], [31]). Biogas can be produced in different

ways, but in this work the focus has been placed on WWTPs installation. The motivation of the study comes in part from the great results of the DEMOSOFC project, the first European example of fuel cell cogeneration plant fed by biogas in a WWTP located in Collegno (TO, Italy) ([32], [33]). The system consists of three SOFC modules of 58 kW AC each, funded by the Fuel Cell and Hydrogen 2 Joint Undertaking under the frame of Horizon 2020 program [34]. Several studies about SOFC modules installation in WWTP have been published, because the possibility to use waste source (i.e. sludge) in order to produce a valuable product (i.e. biogas) through Anaerobic Digestion, it is an opportunity to produce a hydrocarbon fuel in a renewable way ([35]–[38]). For example, according to the International Energy Agency, the bioenergy is the largest source of growth in renewable consumption over the period 2018-2023 [39] and the biogas production from AD belongs to this category. Moreover, this case study can be easily extended to other biogas sources like biomass from farms or OFMSW treatment plants. The Argonne National Laboratory in 2015 provided an overview of the WWTPs and sludge treatment in the US, showing how this fields has still a margin of improvement in the use of the biogas (if produced) and how important is the potential if various feedstocks, with different biogas yield, were used [40].

## 1.4. Tri-generation concept

All the features described so far, regarding the hydrogen need but using high efficiency device like a fuel cell fed by renewable fuel because it comes from waste, lead to the tri-generation concept on HTFC. The interest in this solution depends on the efficient conversion on biogas into power, heat, and hydrogen on a distributed scale as demonstrated by several authors ([41]–[43]). It means that with a single device, in a precise working condition, the tri-generating HTFC faces up all the necessity described earlier (e.g. hydrogen production at lower cost, clean power system, use of bioenergy instead of fossil fuels). Since the hydrogen cost is directly proportional to the efficiency in its production, the technology would be the perfect starting point for the development of hydrogen distributed infrastructure because it is the most efficient means to produce and deliver hydrogen amongst those means considered as conventional technologies [21].

Therefore, this study can be interpreted as the perfect link between DEMOSOFC experience, and the OCSD plant where the first tri-generation MCFC produced by FuelCell Energy® was installed in past years [44]. Running a fuel cell in tri-generation mode means imposing a low utilization factor (e.g. 0.6 instead of the standard 0.8/0.85) in order to process more fuel inside the anode compartment and exploiting the DIR of the cell to exit the cell with a higher concentration of hydrogen. Besides the general advantages in efficiencies that usual polygeneration plants have, the winning point of this solution consists in the fact that lowering the utilization factor, (1) the additional endothermic reformation due to SMR cools down the cell reducing the power associated with the air cooling, (2) the operating voltage increase because of Nernst equation (see chapter 2 for more details) and (3) the heat due to the irreversibility is directly converted in a third product which the hydrogen [45]. The residual heat for cogeneration is still available. Lowering too much the fuel utilization factor means processing more fuel and consequently it increases the heat demanding for SMR, whereas the fuel cell moves from an exothermic towards an endothermic behavior [46]. Another important aspect regards the on-demand feature of this kind of plant, because if they can work in different conditions, they can regulate the hydrogen production according to its demand, saving capital cost on the storage subsystem.

## 1.5. Goal and thesis outline

The only drawback of this application concerns the dynamic operation of the SOFC with internal reforming, because the endothermicity of the SMR will cause a temperature drop in the first part of the cell whereas in the last part, where the electrochemical reaction of the hydrogen dominates, the exothermicity will rise the temperature. This temperature profile into the PEN layer of the cell needs to be evaluated, especially in the dynamic operation when the operating condition of the cell changes. For this reason, a dynamic spatially resolved model is required to understand which are the main concerns in terms of concentrations, temperature, and thermal gradient inside the cell and the difference with respect to the conventional condition in cogeneration mode or with combined power and hydrogen production solved with a lumped parameter model [47](Figure 2).

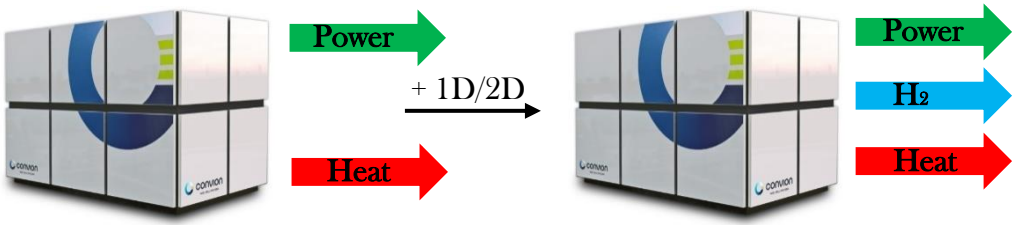


*Figure 2. Spatially resolution in tri-generation and under dynamic condition needed.*

The structure of the work is divided as follow:

- Chapter 2: Description of the model main features;
- Chapter 3: Results of the SOFC stack mainly in tri-generation mode;
- Chapter 4: Fuel cell results are integrated in the dynamic system where performance indexes and methodologies are illustrated;
- Chapter 5: Considerations about two case studies: OCSD and DEMOSOFC.
- Chapter 6: What's next? What's now? Distributed infrastructure in Italy for hydrogen use.

# 2. Model

In order to perform the simulations concerning the tri-generation system, and in particular the behavior of the SOFC, a dynamic and spatially resolved model is required. The Matlab® tool used in this work has been developed at the National Fuel Cell Research Center (NFCRC) at the University of California, Irvine (UCI) along several years [48] and it has been modified in some parts by the author, for the specific purpose of the tri-generation concept. As briefly discussed in the introduction, the necessity of understanding the behavior inside the fuel cell is the main reason of using a quasi-2D (or 3D) model and in the next paragraphs the main features and assumptions of the model will be described.

## 2.1. Solid Oxide Fuel Cell stack

The core of the system, and the component that affects the most the results and the study of this work, is the SOFC. Since the computational effort to solve problems which involve different physics phenomena is important, a good model should find the optimal trade-off between reliable representation of the reality and reasonable computational cost. The fuel cell stack is made of several cells, and each of them can be discretized into five different sub components:

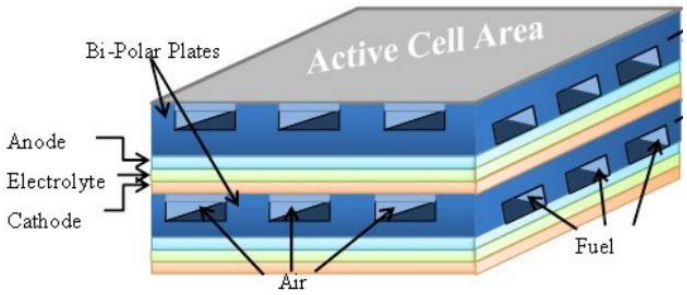


*Figure 3. Fuel Cell repeating unit and CV description in McLarty [1].*

This division is necessary because in each layer, different equations should be imposed. The interconnector plates (or bi-polar plates) are mainly made of metal (stainless steel or graphite) and they have many functions, such as distribute the reactants along the active area via flow channels, being the electrical mean to carry the current among the cells and allow the heat conduction across the cell for a better heat transfer. At the same time, they should be chemically very stable in both anodic and cathodic environments with very low gas permeability.

The anodic channel is one of the two channels in contacts with the interconnector and the PEN (Positive-Electrolyte-Negative) electrode assembly. In the fuel cell operation, this the fuel flow path where in case of DIR the SMR and WGS occur. The migration of the hydrogen molecules towards the TPB start from this point.

The PEN is the actual layer in which the electrochemical reaction occurs. In the SOFC the electrolyte is a solid layer that allows only the passage of $O^{2-}$ ions from the cathode side to the anode side.

The cathodic channel has two main functions: distribution of the oxygen molecules needed for the electrochemical reaction and remove (or supply) heat from (to) the fuel cell, in order to control its temperature.

### 2.1.1. Computational domain

In order to further reduce the computational domain, without losing any important physical aspects of the phenomenon, the code models the cell in four layers, treating the two bi-polar plates as one single domain but with its proper geometry.

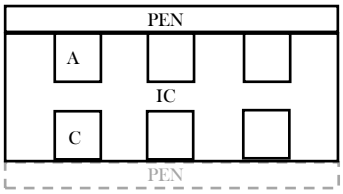


*Figure 4. Computational domain in 4 layers: Interconnector (IC), Anode channel (A), Cathode channel (C), Positive-Eletrolyte-Negative (PEN)*

The only difference is in term of the boundary conditions applied to each section. Then, every layer has been discretized in control volumes in which the different equations for energy and species conservation are applied.

The technique used by McLarty et al. allow the user to run simulation with a discretization with $n$ columns and $m$ rows of the cell area and permits different flow configurations just changing the vector connections outputs to inputs. Moreover, other important assumptions of the model are:

- Perfectly stirred reactor in each gaseous CV
- Temperatures and species are averaged between inlet and outlet

- No edge effect of the fuel cell stack, each cell has the same behavior

As already demonstrated by other authors [48], [49], the grid independence study showed that using a discretization with more than 10 nodes for the fuel cell, will increase the computational cost (especially in the cross-flow configuration) without an appreciable difference in the results. Thus, in this work almost every simulation has been running with 10 nodes, except for a couple of them only for a clearer graphically explanation of the results.

### 2.1.2. Energy and species conservation

The expression of the energy conservation equation applied to each control volume is different for the discretized layers. In the bi-polar plate Eq. (6) there is not heat generation and enthalpy flows, so the only term on the right-hand side of the equation is the $\dot{Q}_T$ term associated with the convective and conductive heat transfer between adjacent nodes (solid-solid) and interface solid-gas with the channels. From equation (7) to (9), the energy equations are presented also for the other three layers:

$$\frac{dT_{IC}}{dt} = \frac{\dot{Q}_T}{\rho_{IC} \cdot c_{IC} \cdot V_{IC}} \tag{6}$$

$$\frac{dT_{an}}{dt} = \frac{\dot{Q}_T + \dot{H}_{in} - \dot{H}_{out} + \dot{Q}_{ion} - \dot{Q}_{react}}{\rho_{an} \cdot c_{an} \cdot V_{an}} \tag{7}$$

$$\frac{dT_{PEN}}{dt} = \frac{\dot{Q}_T + \dot{Q}_{gen}}{\rho_{PEN} \cdot c_{PEN} \cdot V_{PEN}} \tag{8}$$

$$\frac{dT_{ca}}{dt} = \frac{\dot{Q}_T + \dot{H}_{in} - \dot{H}_{out} - \dot{Q}_{ion}}{\rho_{ca} \cdot c_{ca} \cdot V_{ca}} \tag{9}$$

Where $\rho$ is the density [kg/m$^3$] (for the anode and cathode gases, it is computed with the ideal gas law), $c$ is the specific heat capacity [J/kg/K] and $V$ is the volume. In the Eq. (7) and (9) the terms $\dot{H}_{in}$ and $\dot{H}_{out}$ are the total enthalpy [kW] of the anode and cathode flows at the inlet and outlet of each node. $\dot{Q}_{ion}$ represents the sensible enthalpy flow associated with the crossing of the oxygen ions through the electrolyte, from cathode side to anode side:

$$\dot{Q}_{ion} = \frac{I}{4 \cdot F} \cdot h_{s,O_2} \tag{10}$$

The total heat generated by the electrochemical reaction inside the fuel cell is:

$$\dot{Q}_{react} = \frac{I}{2 \cdot F} \cdot \left( h_{H_2} + \frac{1}{2} \cdot h_{O_2} - h_{H_2O} \right) \tag{11}$$

where all the enthalpies have been evaluated at the PEN temperature. However, part of the $\dot{Q}_{react}$ is transformed in electrical power through the electronic flow coming from the hydrogen dissociation in the TPB. Therefore, the actual heat that increases the temperature of the fuel cell (or the heat that should be removed in order to keep the temperature constant) is:

$$\dot{Q}_{gen} = \dot{Q}_{react} - P = \dot{Q}_{react} - V \cdot I \tag{12}$$

Since the model uses the total enthalpy in the energy balance, the heat absorption and production due to the SMR and WGS respectively are already taken into account in those enthalpy terms because the composition of the flow is changing in each node. However, since one of the main parameters that will affect the study of the tri-generation mode of the fuel cell is the total exothermicity of the device, the contribution of the SMR and WGS have been into consideration separately:

$$Exothermicity = EXO = \dot{Q}_{gen} - \dot{Q}_{SMR} - \dot{Q}_{WGS} \tag{13}$$

As previously discussed, the SMR is a strongly endothermic reaction ($\dot{Q}_{SMR} > 0$) whereas the WGS reaction is slightly exothermic ($\dot{Q}_{WGS} < 0$), so the net thermal load of the cell is expressed by Eq. (13). Keeping track of this parameter, it is easy to understand in which conditions the fuel cell is operating, mainly according to the fuel utilization factor because when the EXO>0 the cell is exothermic and so a cooling mass air flow is needed in order to keep constant the temperature. While the heat associated to the electrochemical reaction has been evaluated at the PEN temperature, for the reforming and shift reactions, the temperature used in the enthalpy calculation is the one of the anode channels. The enthalpy calculation uses Shomate equation with coefficients taken from NIST's online chemistry Webbook [50].

Concerning the convection inside the fuel cell channels, the assumption is a fully developed flow, assuming a constant Nusselt number [51]:

$$Nu = \frac{h_{conv} \cdot D_h}{k} = 4 \tag{14}$$

In this way the fluid dynamic problem is simplified, allowing the calculation of the $h_{conv}$ knowing the properties and geometry of the system in terms of $k$ conductivity of the gas (fuel and air) and the $D_h$ hydraulic diameter of the channels.

Since one of the goals is to study the dynamic performance and response of the system, and of the fuel cell itself, a bunch of other properties are needed and retrieved from literature:

| Element | Parameter | Value | Unit | Ref. |
|---|---|---|---|---|
| Cell | Length | 0.09 | m | [29] |
| | Width | 0.09 | m | [29] |
| IC | Thickness | 0.00128 | m | [29] |
| | Density | 1975 | kg/m$^3$ | [51] |
| | Specific heat | 611 | J/kg/K | [51] |
| | Conductivity | 25.23 | W/m/K | [51] |
| Anode channel | Height | 0.0018 | m | |
| | Width | 0.0055 | m | |
| | Wall thickness | 0.002 | m | [51] |
| Cathode channel | Height | 0.0018 | m | |
| | Width | 0.0055 | m | |
| | Wall thickness | 0.002 | m | [51] |
| Electrolyte | Membrane thick. | 8e-6 | M | [29] |
| | Cathode thick. | 30e-6 | m | [29] |
| | Anode thick. | 240e-6 | m | [29] |
| | Density | 375 | kg/m$^3$ | [51] |
| | Specific heat | 800 | J/kg/K | [51] |
| | Conductivity | 6.19 | W/m/K | [51] |

*Table 1. Solid Oxide Fuel Cell parameters used in the work*

The mass balance is the other equation that must be verified for each node, but since the composition of the two gaseous flow is changing along the channel it is better to express the conservation of the mass for all the species involved in the model. The model works with a finite number of species, specified by the user, and in this work, it is possible to distinguish the fuel composition with the air composition:

Fuel = [$CH_4$ CO $CO_2$ $H_2$ $H_2O$ $N_2$]

Air = [$N_2$ $O_2$]

In this way it is possible to run simulation with different fuel composition, from pure or humidified hydrogen to biogas, exploiting one of the main advantages about the supply flexibility of the fuel cell. In the anode side:

$$\frac{d\chi_{CH4}}{dt} = [(\dot{n}_{an} \cdot \chi_{CH4})_{in} - (\dot{n}_{an} \cdot \chi_{CH4})_{out} - SMR] \cdot \frac{R \cdot T_{an}}{p_{an} \cdot V_{an}} \quad (15)$$

$$\frac{d\chi_{CO}}{dt} = [(\dot{n}_{an} \cdot \chi_{CO})_{in} - (\dot{n}_{an} \cdot \chi_{CO})_{out} + SMR - WGS] \cdot \frac{R \cdot T_{an}}{p_{an} \cdot V_{an}} \quad (16)$$

$$\frac{d\chi_{CO2}}{dt} = [(\dot{n}_{an} \cdot \chi_{CO2})_{in} - (\dot{n}_{an} \cdot \chi_{CO2})_{out} + WGS] \cdot \frac{R \cdot T_{an}}{p_{an} \cdot V_{an}} \quad (17)$$

$$\frac{d\chi_{H2}}{dt} = \left[(\dot{n}_{an} \cdot \chi_{H2})_{in} - (\dot{n}_{an} \cdot \chi_{H2})_{out} + 3 \cdot SMR + WGS - \frac{I}{2 \cdot F}\right] \cdot \frac{R \cdot T_{an}}{p_{an} \cdot V_{an}} \quad (18)$$

$$\frac{d\chi_{H2O}}{dt} = \left[(\dot{n}_{an} \cdot \chi_{H2O})_{in} - (\dot{n}_{an} \cdot \chi_{H2O})_{out} - SMR - WGS + \frac{I}{2 \cdot F}\right] \cdot \frac{R \cdot T_{an}}{p_{an} \cdot V_{an}} \quad (19)$$

$$\frac{d\chi_{N2}}{dt} = [(\dot{n}_{an} \cdot \chi_{N2})_{in} - (\dot{n}_{an} \cdot \chi_{N2})_{out}] \cdot \frac{R \cdot T_{an}}{p_{an} \cdot V_{an}} \quad (20)$$

Likewise, in the cathode side the only species that changes is the $O_2$ which react after crossing in forms of ions the solid electrolyte layer:

$$\frac{d\chi_{O2}}{dt} = \left[(\dot{n}_{cat} \cdot \chi_{O2})_{in} - (\dot{n}_{cat} \cdot \chi_{O2})_{out} - \frac{I}{4 \cdot F}\right] \cdot \frac{R \cdot T_{cat}}{p_{cat} \cdot V_{cat}} \quad (21)$$

$$\frac{d\chi_{N2}}{dt} = [(\dot{n}_{cat} \cdot \chi_{N2})_{in} - (\dot{n}_{cat} \cdot \chi_{N2})_{out}] \cdot \frac{R \cdot T_{cat}}{p_{cat} \cdot V_{cat}} \quad (22)$$

From Eq. (15) to (22), the $\dot{n}$ is the molar flow rate referring first to the anode flow (fuel) and then to the cathode flow (air). The species molar fraction is expressed

by $\chi$ and $p, V$ and $T$ are pressure, volume and temperature respectively of the anode and cathode flow. $R$ is the universal gas constant.

When the fuel supplied to the SOFC contains hydrocarbons such as methane and carbon monoxide (e.g. biogas), the SMR and WGS reactions occur in the anode side and then these two terms appear in the species balance. The electrochemical reaction consumes hydrogen and oxygen producing water vapor, so the term $\frac{I}{zF}$ comes from the Faraday's law of electrolysis, where $I$ is the current, $z$ is the number of electrons involved in the reactions (i.e. 2 for each $H_2$ and 4 for $O_2$) and $F$ is the Faraday's constant.

### 2.1.3. Kinetics

Usually, there are several approaches to calculate the rate of SMR and WGS.

The first one is the equilibrium model, in which both the reforming and water gas shift reach equilibrium in the cell thanks to the high temperature in the anodic channel [52]. In this case the local composition in each node of the cell is calculated by the equilibrium constants.

Even though the equilibrium model is suitable to represents a 0-D model, evaluating the fuel cell only in terms of global performance, with the spatially resolved model a second approach that uses kinetics model is preferable. The main reason is that SMR kinetics are slower than WGS and electrochemical oxidation, so the equilibrium could not be reached in a finite domain. Moreover, the main changes in temperature and concentrations verified in the first half of the cell, near the fuel inlet, where the main drop in temperature occur [53]. When the methane content finishes, the main reaction will be the electrochemical one, stabilizing both temperature and concentrations along the rest of the cell.

Different kinetics expressions have been analyzed in last decades, and the studies can be grouped in three different categories according to which type of kinetic expression is used: general Langmuir-Hinshelwood kinetics, first order reaction with respect to methane and power law expressions from data fitting [25]. As explained in Dam-Johansen et al., the first order reaction in methane is a valid choice for 2D/3D models which examine changes in composition and

temperature inside the gas channels but avoiding excessive computations such as the micromodels that describe in detail the electrode physics. For this reason, the most widely used expression by Achenbach and Riensche [54] has been used in this model:

$$\dot{r}_{CH_4} = k_{CH_4} \cdot p_{CH_4} \cdot \exp\left(-\frac{E_{CH_4}}{R \cdot T}\right) \tag{23}$$

Where the activation energy of the methane is 82 kJ/mol [55]. Concerning the WGS reaction, the equilibrium expression is still a valuable choice and the equilibrium constant is determined by.

$$k_{WGS} = \exp\left(-\frac{\Delta G}{R \cdot T}\right) \tag{24}$$

### 2.1.4. Electrochemistry

In literature, there are different models concerning the electrochemical calculation. First, the main assumption of the current model is the equipotential surface constraint across the cell, ensuring that the voltage of the cell is unique, and it allows the recalculation of the current density at each time step starting from the set point (guess) value defined by the user.

After specifying a guess value for the current density, and the rated power of the fuel cell, at each time step the current can be calculated and from that value the fuel flow necessary to produce that current and voltage via Faraday's law of electrolysis:

$$n_{fuel} = \frac{I}{2 \cdot F \cdot U_f \cdot (4 \cdot \chi_{CH_4} + \chi_{CO} + \chi_{H_2})} \cdot n_{cells} \tag{25}$$

Where the $U_f$ is the utilization factor defined as:

$$U_f = \frac{H_{2.consumed}}{H_{2.available}} \tag{26}$$

In each node of the discretization, the local reversible voltage is computed from the ideal standard potential for the cell reaction $E_0$ and the effects of temperature and partial pressures of reactants and products, as defined by the Nernst potential:

$$V_{Nernst} = E_0 + \frac{R \cdot T_{PEN}}{2 \cdot F} \cdot \ln\left(\frac{p_{H_2} \cdot {p_{O_2}}^{\frac{1}{2}}}{p_{H_2O}}\right) = \\ = -\frac{\Delta\overline{g_0}}{2 \cdot F} + \frac{R \cdot T_{PEN}}{2 \cdot F} \cdot \ln\left(\frac{p_{H_2} \cdot {p_{O_2}}^{\frac{1}{2}}}{p_{H_2O}}\right) \quad (27)$$

Where $\Delta\overline{g_0}$ is the molar Gibbs free energy of the electrochemical reaction in standard condition and evaluated at the nodal PEN temperature. The partial pressures $p_i$ refer to the hydrogen and steam in the anode channel and the oxygen in cathode one. Since the total pressure is different from the two channels, the expression in the logarithmic term may be expressed with the species molar fractions and the square root of the cathode pressure.

In order to calculate the actual voltage, three additional losses should be added to the Nernst voltage:

$$V_{cell} = V_{Nernst} - \eta_{act} - \eta_{ohm} - \eta_{diff} \quad (28)$$

In general, for HTFC the ohmic loss is responsible for the main drop in voltage from the $V_{Nernst}$ because the high temperature and the typical current densities at which the fuel cell operates produce small activation and diffusion losses. However, in this model both the $\eta_{act}$ and $\eta_{diff}$ have been considered for two reasons: since the internal reforming causes a temperature drop near the entrance of the fuel flow, and the activation loss is strongly related to the temperature as described in the Eq. (29) in some condition they are not negligible; the reason for considering the diffusion loss is that different operating conditions with different fuel compositions will be investigated, so cautiously the case in which the reactant concentration in the catalyst layer drops to zero should be taken into account, especially in at the two ends of the cell. Here a more detailed explanation:

$$\eta_{act} = \frac{R \cdot T_{PEN}}{F} \cdot \sinh^{-1}\left(\frac{j}{2 \cdot j_{0,an}}\right) + \frac{R \cdot T_{PEN}}{F} \cdot \sinh^{-1}\left(\frac{j}{2 \cdot j_{0,cat}}\right) \quad (29)$$

$$j_{0,an} = \gamma_{an} \cdot \left(\frac{p_{H_2}}{p_{amb}}\right) \cdot \left(\frac{p_{H_2O}}{p_{amb}}\right) \cdot \exp\left(-\frac{E_{act,an}}{R \cdot T_{PEN}}\right) \quad (30)$$

$$j_{0,cat} = \gamma_{cat} \cdot \left(\frac{p_{O_2}}{p_{amb}}\right)^{0.25} \cdot \exp\left(-\frac{E_{act,cat}}{R \cdot T_{PEN}}\right) \quad (31)$$

The Eq (29) is called Butler-Volmer equation, when the electronic transfer coefficient (also called symmetry factor) is equal to 0.5. The expression of exchange current density $j_0$ is given by Eq (30,31) [56]. The values of the pre-exponential factors, the activation energy $E_{act}$ as well as other parameters are listed in Table 2. The choice of defining a temperature dependent exchange current density has been demonstrated to be more accurate with experimental results than assuming constant values [57].

The ohmic loss has two main contributions: electrolyte, strongly dependent from the temperature and interconnector.

$$\eta_{ohm} = j \cdot \left[\frac{t^M \cdot T_{PEN}}{A \cdot \exp\left(-\frac{\Delta G_{act}}{R \cdot T_{PEN}}\right)} + R_{IC}\right] \quad (32)$$

Where $t^M$ is the membrane thickness and $A$ is the electrolyte constant [28]. The $R_{IC}$ is the additional constant resistance due to the interconnections in the whole stack [58].

The other loss that remains to be found is the diffusion loss (or concentration):

$$\eta_{diff} = \frac{R \cdot T}{z \cdot F} \cdot \ln\left(\frac{j_l}{j_l - j}\right) \quad (33)$$

Where $z$ is equal to 2 or 4 if refers to anodic or cathodic contribution respectively. The expression of the limiting current density $j_l$, that is the maximum current density the fuel cell can sustain because at that current the concentration of the reactants falls to zero, is given by Eq (34):

$$j_l = z \cdot F \cdot D_i^{eff} \cdot \frac{C_{bulk,i}}{\delta} \quad (34)$$

The previous equation is valid both for the anodic and cathodic limiting current density, where $\delta$ is the thickness of the layer and $C_{bulk,i}$ is the species concentration in the bulk stream, whereas the $D_i^{eff}$ is the effective diffusion coefficient.

| Parameter | Variable | Value | Units |
|---|---|---|---|
| Activation energy, AN | $E_{act,an}$ | 1e5 [57] | kJ/kmol |
| Activation energy, CAT | $E_{act,cat}$ | 1.17e5 [57] | kJ/kmol |
| Pre-exponential factor, AN | $\gamma_{an}$ | 1.344e10 [57] | A/m$^2$ |
| Pre-exponential factor, CAT | $\gamma_{cat}$ | 2.051e9 [57] | A/m$^2$ |
| Electrolyte activation energy | $\Delta G_{act}$ | 100 [51] | kJ/kmol |
| Electrolyte constant | $A$ | 13e7 [51] | K/Ω/m |
| Eff. Oxygen diffusivity | $D_{O_2}^{eff}$ | 2.0e-5 [28] | m$^2$/s |
| Eff. Hydrogen diffusivity | $D_{H_2}^{eff}$ | 1.0e-4 [28] | m$^2$/s |

*Table 2. Electrochemical model parameters*

## 2.2. Balance of Plant components

The model description will be completed in this section, with the main features and assumptions for the balance of plant components.

### 2.2.1. Heat Exchangers

The reason of modelling the heat exchanger not as bulk model but at least in 1D (for the HXs involved in the dynamic simulation) is to be sure that in the dynamic and off-design conditions there are no temperature crosses in them. The simplicity of the model assumes three layers (Cold fluid, Solid layer, Hot fluid) with a space discretization and allow both counter and co-flow configurations. The counterflow has been chosen. The solid plate is subjected to the convective heat transfer with the two flows and the conduction inside the plate itself:

$$\frac{dT_{H,C}}{dt} = \frac{\dot{Q}_{T,H,C} + \dot{H}_{in,H,C} - \dot{H}_{out,H,C}}{\frac{V_{H,C} \cdot p_{H,C} \cdot c_{p_{H,C}}}{T_{H,C} \cdot R}} \tag{35}$$

$$\frac{dT_{solid}}{dt} = \frac{\dot{Q}_{T,solid}}{V_{solid} \cdot p_{solid} \cdot c_{solid}} \tag{36}$$

The term $\dot{Q}_T$ considers the heat transfer in the different layer, and so is different from Eq (35) to (36) because of the different heat exchange mechanisms involved, as already clarified. For a more detailed explanation about the possible flow configurations and vector organization in the code, it is suggested to investigate the source further [48].

| Parameter | Variable | Value | Units |
|---|---|---|---|
| Number of nodes | $n$ | 10 | - |
| Convective HTC | $h_{conv}$ | 50 | W/m$^2$/K |
| Plate thickness | $t_{HX,plate}$ | 0.001 | m |
| Plate specific heat | $c_{p,plate}$ | 480 | J/kg/K |
| Plate conductivity | $k_{plate}$ | 15 | W/m/K |
| Plate density | $\rho_{plate}$ | 8055 | kg/m$^3$ |

*Table 3. Heat Exchangers (dynamic model) parameters*

### 2.2.2. Blower

In order to regulate the air flow on the cathode side, mainly to control on of the set point of the fuel cell that will be discussed in the next chapter, a blower is required to overcome all the pressure drops on the air line. To determine the shaft velocity the model uses the dynamic shaft torque balance, governed by the Eq (37) [59].

$$\frac{dw}{dt} = \frac{P_{blower} - P_{impeller}}{J \cdot w} \tag{37}$$

Where the dynamic variable is the speed $w$ and $J$ is the moment of inertia. When the difference between the power supplied to the blower $P_{blower}$ and the power required to compress the mass flow needed $P_{impeller}$ is positive, the shaft is increasing its speed otherwise the derivative will be negative. The power required for the compression is:

$$P_{impeller} = \frac{\dot{V}_{air} \cdot (p_{out} - p_{in})}{\eta_{blower}} \tag{38}$$

### 2.2.3. Oxidizer

This component model a complete combustion, if enough oxidant is provided, simulating three oxidation reactions:

$$CH_4 + \frac{3}{2} O_2 \rightarrow CO + 2H_2O \tag{39}$$

$$CO + \frac{1}{2} O_2 \rightarrow CO_2 \tag{40}$$

$$H_2 + \frac{1}{2} O_2 \rightarrow H_2O \tag{41}$$

In a similar logic to the other components, the mass and energy balance applied. Useful outcomes from this component are the outlet temperature and the total molar flow of the exhaust because they can be used to estimate the available heat for co-generation, once the efficiency of the combustor is defined.

$$\frac{dT_{out}}{dt} = \frac{H_{in} - H_{out}}{V_{ox} \cdot c_p \cdot p_{in}} \cdot T_{out} \cdot R \tag{42}$$

Another important parameter regarding this component, is the fuel-air equivalence ration of the mixture of the combustion which is expressed by Eq (43), and it will affect strongly the temperature of the exhaust.

$$\varphi = \frac{n_{fuel}/n_{ox}}{(n_{fuel}/n_{ox})_{st}} = \frac{n_{ox,st}}{n_{ox}} \tag{43}$$

The more the equivalence ration is closer to 1, the more the mixture is close to the stochiometric combustion and the temperature will be the highest. For $\varphi > 1$ the oxidizer will deal with a rich mixture, instead for values $\varphi < 1$ the mixture is poorer.

In the paragraph 2.4.3, the oxidizer behavior will be discussed in detail concerning one of the possible regulations of the plant.

### 2.2.4. Connections and states

One of the advantages of the EAGERS code is the modularity. Even though completely written in Matlab® and without GUI, the logic behind the connection among different components is a breakthrough. Each component has its own input and output in terms of flow, temperature, power, and pressure. This latter parameter allows the code to construct an entire flow that start supposedly from a source and it ends up in the atmosphere or as product. The change in pressure across the line is computed backwards adding for each component a certain pressure drops defined by the user (or suggested by the author of the code). In some point there could be ramifications of flows (e.g. split, three-way valve, bypass, separation of products) and in that case the component with more than one outlet, must be connected to the same number of other components, or the environment.

Once defined the complete system that the user wants to simulate dynamically, all the components that have "states" will be simulated step by step. The states are the variables that need to be solved through the governing equations of the model, thanks to the ODEsolver: this approach is called State-space modeling, and the equation below shows the form in which they appear with $\dot{x}$ the change in states of the model, and $f$ is the function of the governing equation.

$$\dot{\boldsymbol{x}} = f(\boldsymbol{x})$$

McLarty explained the advantages of solving a vector of states of all the equations of the model instead of solving node by node and component by component every unknown. As an example, looking at the Eq. (8), one of the states of the solid oxide fuel cell is the $T_{PEN}$. If the discretization consists of n nodes, it means that there are n values of $T_{PEN}$ that need to be solved. Then, the variation of the state in this case is represented by $\frac{dT_{PEN}}{dt}$.

## 2.3. Controller logic

Running simulations dynamically implies one main difference from the steady state simulations, that is the necessity of a controller logic in order to react to the perturbations of the system (i.e. of the fuel cell). The way the controller

manipulates some variables is not unique: in this work a PI controller has been used.

Several authors adopted different logics and they used different parameters as error for to be controlled, from the set point required ([51], [59]–[61]). Certainly, the most important parameter for HTFC is the cell temperature because from this value depend many other parameters that affect the performance of the device and the downstream components of the system as well. Another important aspect that should be carefully considered in the high temperature SOFC when operated dynamically is the thermal stresses at which this device is subjected. For example, at least two types of thermal stresses due to temperature gradients must be controlled and bounded: along the direction of the flows, so between the two ends of the PEN layer; thermal expansion in the same point due to thermal cycle, on the direction perpendicular to the cell.

These are the reasons why in this work the $T_{PEN}$ and $\Delta T_{stack}$ have been chosen as variables to be controlled. The errors $e(t)$ associated with these two parameters express the distances from the setpoints defined by the user and the PI controller correction $u(t)$ is expressed by Eq (46), where $K_p$ and $K_I$ are the proportional and integral gains, defined by the user.

$$e_1(t) = \frac{T_{PEN,avg}(t) - T_{PEN,sp}}{\Delta T_{stack,sp}} \tag{44}$$

$$e_2(t) = \frac{\Delta T_{stack}(t) - \Delta T_{stack,sp}}{\Delta T_{stack,sp}} \tag{45}$$

$$u(t) = K_p \cdot e(t) + K_I \cdot \int_0^t e(t') \cdot dt' \tag{46}$$

Once decided the two setpoints for the variables described, the controller needs to act on some physical quantities that are able to change the behavior of the cell according to the error calculated. In general, the temperature control is more important in terms of results and performance of the fuel cell, since it is one of the main driving forces for its thermodynamics and electrochemistry, so only the first regulation could be applied. However, since the use of modeling should be

thought as mean to simulate a real situation, even though there is no mechanical behavior modelled due to thermal expansion inside the SOFC, the control of the $\Delta T_{stack}$ gives more consistency to the model. A further explanation of this choice will be provided in the next section when the whole layout is presented, and the design decisions will be explained.

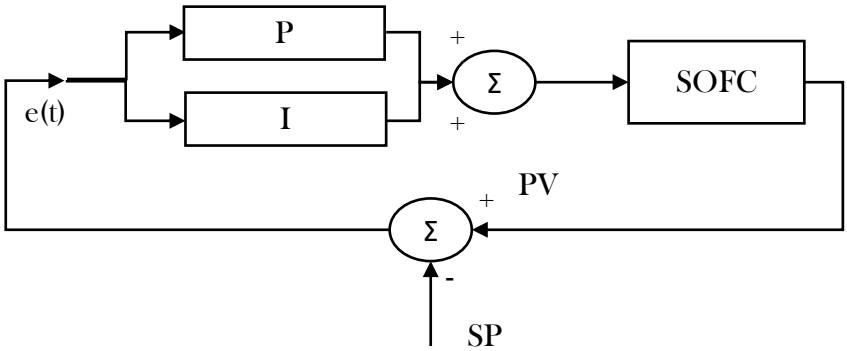


*Figure 5. Controller logic scheme.*

In the Table 4 the setpoint values and other valuable parameters are listed.

| Set point | Value | Units | Controlled by |
|---|---|---|---|
| PEN average temperature | 1023 | K | AirBypass |
| Stack temperature difference | 60-90 | K | AirFlow |
| Lower bound air flow | 2×minimum | kmol/s | |

*Table 4. Set points and constraint used by PI controller*

## 2.4. System Layout

The discussion of the first chapter about the tri-generation plant led to a system layout as depicted in Figure 6. Taking a quick look to the layout, it is clear how the three products are produced: Power from the SOFC, hydrogen production from the HSU, and heat from the co-generation heat exchangers. There are three main lines, illustrated with three different colors, which represent the input of biogas (fuel), water (recovered by the separation unit) and air (from the environment).

The aim of realizing a polygeneration plant suitable for installation in WWTP, and generally suitable for feeding the fuel cell with biogas, has to face different challenges when the dynamic control of the products is required. For this reason,

several assumptions have been done to pursue the main goal of this study, focusing on the SOFC dynamics and its hydrogen production.

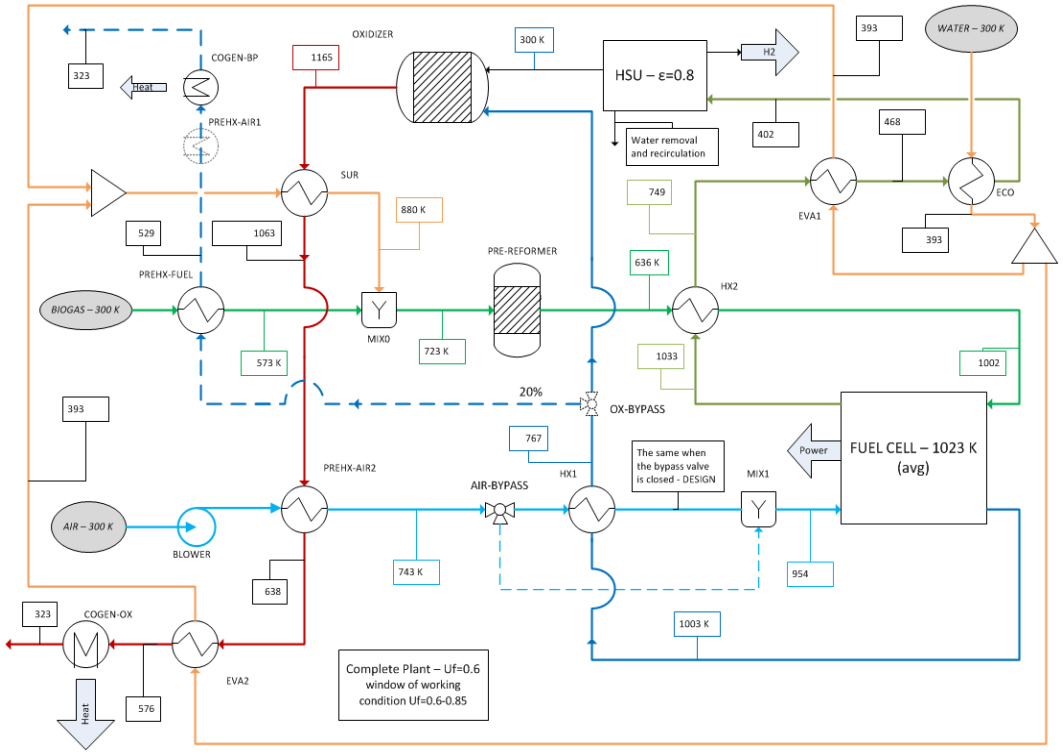


*Figure 6. System layout in the design condition: fuel pipeline in green, air in blue, water in orange and exhaust in red.*

The biogas produced by the Anaerobic Digestion is first sent to the gas holder before the clean-up section. From this point, the blower on the fuel side compresses the biogas that passes through a chiller and very fine clean-up section called biogas processing unit [33]. One more time, since the main goal is to evaluate the dynamic of the fuel cell and of the products that a tri-generation plant can generate, the pre-treatment of the fuel (and the water as well) has not been evaluated. An adiabatic pre-reformer is placed between a mixer used to reach the S/C ratio and the heat exchanger on the fuel line before the inlet of the fuel cell (HX2). The choice of the inlet temperature for the adiabatic reformation will be explained later.

On the air side, two heat exchangers are providing enough temperature for the inlet in the SOFC. The bypass valve, active part in the control of the PEN temperature, can bypass part of the air flow across the heat exchanger (HX1), and

mix it (colder) downstream. The strategy adopted involves the manipulation of the oxidant flow through the blower to control the $\Delta T_{stack}$ and a bypass valve on the air side, to regulate the $T_{PEN}$.

The water line is subjected to quite standard engineering process, reaching the steam condition required for the mix with the fuel before the pre-reformer. An important remark regards the total recovery of the water separated through condensation before the PSA in the HSU, sufficient to close the loop without adding fresh water.

The residual of the HSU (mainly $H_2$, CO) and the depleted air from the outlet of the fuel cell are reacting in the oxidizer, making available additional heat for the preheating and the useful co-generation.

### 2.4.1. Design assumption

The complexity of the whole system required some simplifying assumptions during its definition:

a) Fuel and water processing unit outside the scope of the study
b) Dynamic part is a small part of the plant that involves only main components close to the SOFC
c) The non-dynamic part of the BoP has been resolved with simple calculation (e.g. first law of thermodynamics) and lumped parameter model
d) Arranging the layout without anodic recirculation, for tri-generation purpose ($H_2$ separated in the HSU), to have an higher hydrogen concentration in the anode outlet and enough hydrogen molar flow that needs to be separated.
e) Constant inlet temperature of the fuel flow
*f) Allowing heat recovery with the outlet streams even in tri-generation operation, supposing that the fuel cell is not fully endothermic.*

The last observation has a strong consequence in the design choices. The key point of a tri-generation plant using HTFC is to use a lower fuel utilization factor because it allows to process more fuel flow inside the cell, ending up with a higher

molar fraction of hydrogen at the anode outlet, thanks to the internal SMR and WGS. As the $U_f$ goes down, the endothermic reaction inside the cell has a higher weight on the thermal balance of the cell and the while the temperature profile of the PEN in changing, the temperature of the outlets decrease as well. On one hand, with the lowest possible utilization factor, the production of the hydrogen is maximized. On the other hand, the fuel cell will become more endothermic, and at system level there will be the necessity to supply both inlets at higher temperature than the set point, without possibility to recover heat from the outlets, since they will be colder than the required inlets.

This exothermicity or endothermicity behavior will be a principal point of the future choices and analysis in this work, starting from the sensitivity analysis on the fuel cell stack.

### 2.4.2. Dynamic domain

In Figure 7 the dynamic layout only is sketched. Those components are the core of the whole plant because indirectly the variables used for the setpoints control, and the three products of the tri-generation plant as well (power, heat, hydrogen) are included in them.

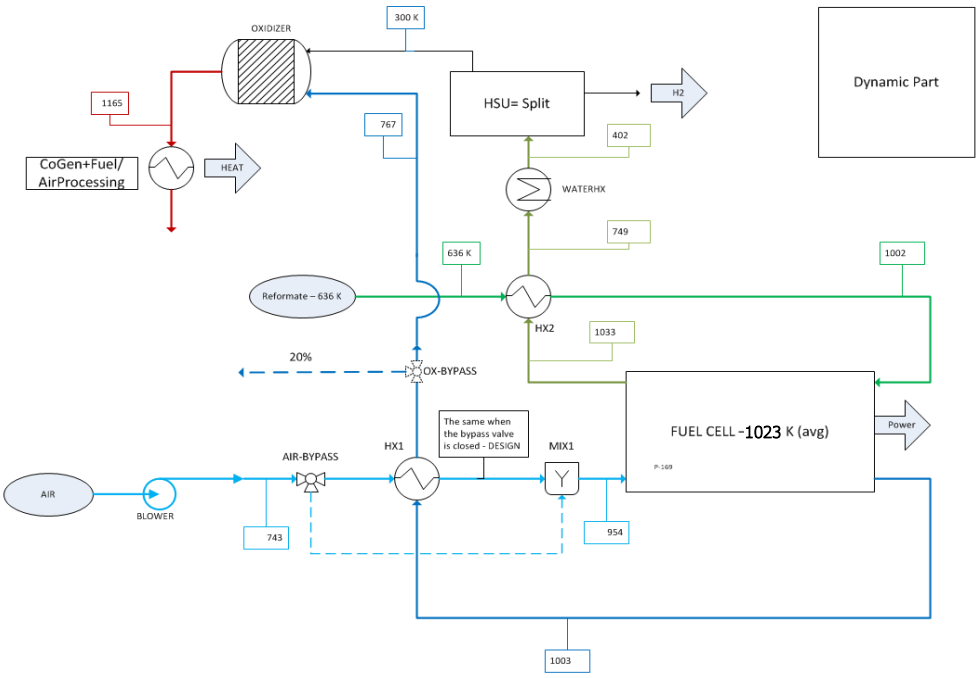


*Figure 7. Domain of the dynamic simulations, design condition*

In this compact view, it is clearer the air flow and bypass control through the blower and three-way valve. In the design condition, described in the next sections, at $U_f = 0.6$, the plant works at the closest operating point to the thermoneutral condition, so it means that the inlet temperature is the highest in the range of utilization factor from 0.6 to 0.85 (co-generation mode). Therefore, when operating in the design condition the air bypass valve is totally closed and all the air flows through the heat exchanger, designed for this condition, and ready to be sent into the cathode channel. As soon the utilization factor is increasing, for example because the hydrogen demand is decreasing, the actuator of the valve is opening the bypass line in order to mix colder air in the mixer right before the fuel cell. In this way colder air is provided to the more exothermic SOFC, and the set point $T_{PEN}$ can be controlled. In the same time, since the cell becomes more exothermic, the cooling load rises, and the mass flow increases as well. The $\Delta T_{stack}$ set point can be seen as a "dynamic set point" in the sense that the maximum value is imposed in the most exothermic case $(U_f = 0.85)$, and it corresponds to a maximum temperature gradient of 90°C over a 9x9 cm cell. The air flow increases, and the bypass valve opens, so the load on the heat exchanger and the following mixing change. If the new steady state at $U_f = 0.85$ will be reached, three out of four temperatures across the SOFC will be changed, and the bypass valve will still be open at certain percentage. This example in changing dynamically the $U_f$ explains how the controller logic works in this situation. Similar behavior when the fuel cell is asked to work in an off-design condition in terms of power bigger than the nominal one.

### 2.4.3. Off-dynamic

This section will focus on two side aspects of the layout, not included in the dynamic simulations.

1. The tri-generation plant uses a SOFC and when an appropriate catalyst is used in the anode layer manufacturing, the DIR occurs when high hydrocarbon content fuel is supplied such as biogas. In this study, the composition of the biogas from the digester has been simplified in only $CH_4$ and $CO_2$ with percentage of 65%/35% respectively and in any case very close to the actual

value coming from the AD in DEMOSOFC, at which this study is inspiring [33], [62]. At the same time, the air composition assumed is 79% $N_2$ and 21% $O_2$. The advantages of the internal reforming have been discussed in Chapter 1, but another aspect is the reduction in capital cost of these systems because they do not need large external reformer and in operational cost because of the necessary heat for its operation. At the same time, the complete internal reforming, that is still possible, may cause issues in the very first part of the fuel cell because of the huge temperature drop that will occur at the entrance of the cell. Especially if the S/C is big enough, the conversion of the methane will be very quick, and as soon the endothermic reaction will be negligible the temperature of the PEN increases a lot due to the electrochemical reaction of the hydrogen just produced by the SMR (and WGS), causing a very important temperature gradient. Besides the problem of the thermal stress, the performance of the fuel cell falls down as well: few simulations demonstrated how the "cold" entry of the cell, causes an important increase of the ohmic and activation losses, and at the same rated power the efficiency is affected by the lower voltage. A very unstable situation in terms of current density in the very first nodes of the cell were also experienced. Moreover, when dealing with pure natural case or even biogas, there will be no hydrogen ready to react at the very beginning of the cell, and the minimum S/C to avoid the carbon deposition could be not enough. To solve, or limit, these issues an external adiabatic pre-reformer has been adopted. At this point the mixture composition and its temperature should be defined at the inlet of the pre-reformer because the yield of the reformation process in the adiabatic reformer depends mostly by the temperature inlet (and the residency time in the reactor). For this reason, different equilibrium compositions of the reformate have been evaluated at different inlet temperature and the compositions downstream the pre-reformer are summarized in Table 5 with the name of reformate case referring to the temperature in °C before the reformation (the first column refers to pure biogas and steam in a mixture of S/C=2).

| Conversion CH4 | 0 % | 8 % | 10 % | 13 % | 16 % |
|---|---|---|---|---|---|
| Name | Fuel 65/35 | Fuel 450 | Fuel 500 | Fuel 550 | Fuel 600 |
| CH4 | 28.2% | 25.1% | 24.1% | 23.1% | 22.0% |
| CO | 0.0% | 0.1% | 0.3% | 0.4% | 0.6% |
| CO2 | 15.2% | 16.5% | 16.8% | 17.1% | 17.4% |
| H2 | 0.0% | 8.0% | 10.4% | 12.9% | 15.4% |
| H2O | 56.5% | 50.3% | 48.4% | 46.5% | 44.6% |
| N2 | 0.0% | 0.0% | 0.0% | 0.0% | 0.0% |

*Table 5. Reformate cases: stream concentrations after pre-reformation. The name Fuel 65/35 stays for 65% methane and 35% carbon dioxide, whereas the other names refer to the inlet temperature in °C of the pre-reformer. The conversion % of methane refers to the relative difference with the case Fuel 65/35*

The choice has been made in order to minimize the heat required for the fuel processing, supposing constant the inlet temperature at the anode. In this way it has been possible to fix the final condition and according to the condition upstream the reformer it comes out that for the reformate at 8% of conversion in terms of $CH_4$ the lowest amount of heat is required. Even though the specific heat changes in the different cases, the main reason that led to the previous conclusion is that the difference in temperature across the pre-reformer is neither constant nor linear, as showed in the last column of Table 6.

| Reformate | Heat Load [kW] | Fuel molar flow [kmol/s] | $\Delta T_{reformer}$ [K] |
|---|---|---|---|
| 450 | 32.36 | 5.64e-4 | -87 |
| 500 | 33.93 | 5.71e-4 | -114 |
| 550 | 35.51 | 5.77e-4 | -144 |
| 600 | 37.28 | 5.85e-4 | -175 |

*Table 6. Evidence of the heat required for processing the reformate.*

The amount of heat required for the steam is not included in the analysis because the specific heat is the same and for higher inlet temperature corresponds a higher temperature of steam production, so it means that for sure the lowest temperature inlet is also the one that required the least energy for the steam supply. The amount of heat needed by the required steam is directly proportional with the inlet temperature of the mixture in the reformer.

In any case, preliminary simulations have been conducted with each of those reformates in order to catch the main differences in performances of the fuel cell. The most relevant results are shown in the Table 7.

| Name<br>Conversion of CH4 | bio<br>0% | 450<br>8% | 500<br>10% | 550<br>13% | 600<br>16% |
|---|---|---|---|---|---|
| Air in temperature [K] | 992.0 | 955.7 | 944.1 | 945.3 | 946.7 |
| Air flow [kmol/s] | 1.70E-03 | 1.74E-03 | 1.77E-03 | 2.11E-03 | 2.52E-03 |
| Fuel flow [kmol/s] | 5.42E-04 | 5.64E-04 | 5.71E-04 | 5.77E-04 | 5.85E-04 |
| Exothermicity [kW] | 1.74 | 3.86 | 4.60 | 5.22 | 5.96 |
| Voltage [V] | 0.818 | 0.819 | 0.820 | 0.822 | 0.824 |
| Max dT/dx [K/mm] | 734.07 | 663.98 | 634.67 | 600.60 | 565.55 |
| $H_2$/Fuel | 0.340 | 0.327 | 0.323 | 0.319 | 0.315 |
| Efficiency | 47.2% | 46.6% | 46.3% | 46.2% | 46.0% |

*Table 7. Sensitivity analysis of the reformate cases. Results showed different performance of the cell. The utilization factor is 0.6 and the PEN temperature is 1023 K.*

It is clear from the table above that also in terms of performance, the reformate with less percentage of conversion is the most efficient (as already foreseen by the advantages of DIR). Indeed, at the same rated power, the efficiency of the case 450 is higher than the other cases consuming a less amount of fuel flow. Moreover, the air flow required to cool down the fuel cell is the smallest one because the exothermicity of the cell increases as the percentage of the reformation increases. There are only two drawbacks associated with this choice, but they are not relevant: first, the voltage is 0.819 V in the case 450 whereas is 0.824 in the case 600; second, the air temperature at the inlet of the fuel cell needs to be higher, since the cell is less exothermic but the PEN temperature set point of the must be reached in any case. The exothermicity item, is directly proportional to the % of methane converted, because it means that the endothermic weight of the SMR is smaller inside the fuel cell (Figure 8). Instead the ratio between the hydrogen flow available at the exit and the molar flow of fuel needed in that case provides a better result if pure biogas was used.Flows required to the SOFC and normalized to the Fuel450 case (8%of CH4 reformation).

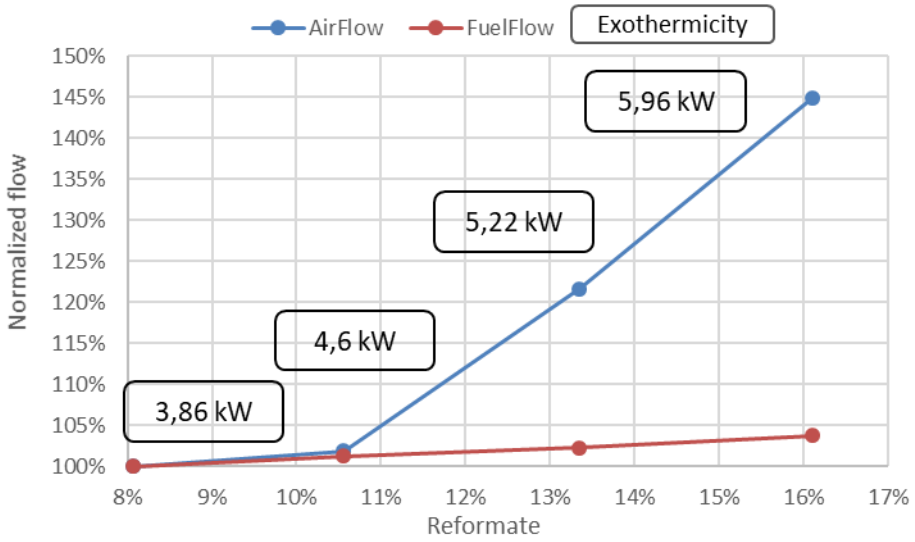


*Figure 8. Flows required to the SOFC and normalized to the Fuel450 case (8%of CH4 reformation).*

2. The best expectation in the design of a polygeneration plant is to define a control system able to control every single product that comes out of the plant. Even though it is very challenging to regulate independently each product, in the design of this system hydrogen and heat production can be handled separately from the power production of the SOFC. Instead, the power control affects unavoidably the other two products because downstream of the SOFC. In the paragraph 4.3, some results of this regulation *a posteriori* is illustrated. Before discussing those simple controls, design conditions should be individuated and for this reason two sensitivity analysis have been carried out of the oxidizer and HSU. In particular, the hydrogen production can change only if the efficiency of the HSU changes (or in general reusing part of the $H_2$ separated) whereas the heat available from the exhaust of the oxidizer could change both for the outlet stream temperature and mass flow. For the HSU regulation, which is not modelled but thought as a common PSA unit, the percentage of hydrogen recovered with respect to the inlet stream in the block is the only parameter.

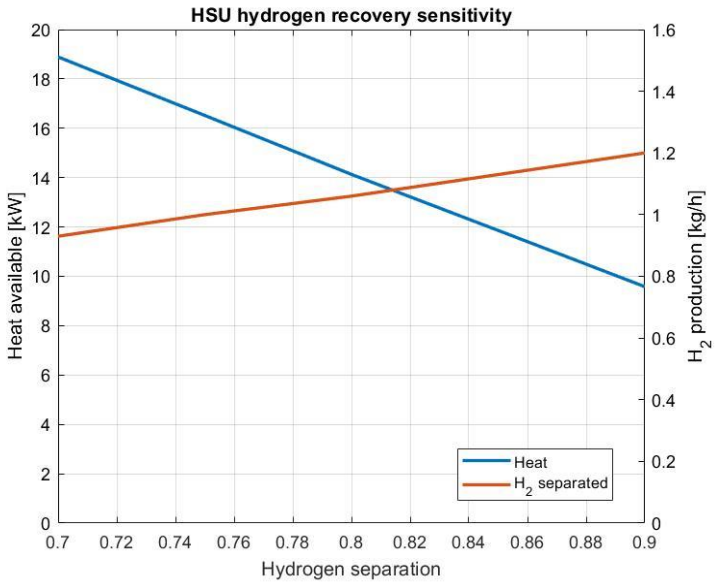


*Figure 9. HSU recovery sensitivity. Design condition at 0.8 (efficiency assumption).*

Clearly, when the percentage increases (up to a maximum of 0.9) it means that more hydrogen is available as final product, but in the meanwhile the molar fraction of hydrogen in residues for combustion is lower and with the same oxidant flowrate (sensitivity analysis only on the HSU) the equivalence ratio is lower, producing an exhaust flow at lower temperature (and in this case even lower thermal power available). The total mass flow is also changing, but the effect is not so important as the one in terms of temperature.

Concerning the oxidizer sensitivity, the main regulation can be done on the incoming pipeline of air to the oxidizer: bypassing a certain amount of air, the equivalence ration can be raised up producing a hotter outlet stream but reducing the total flow and eventually the available heat.

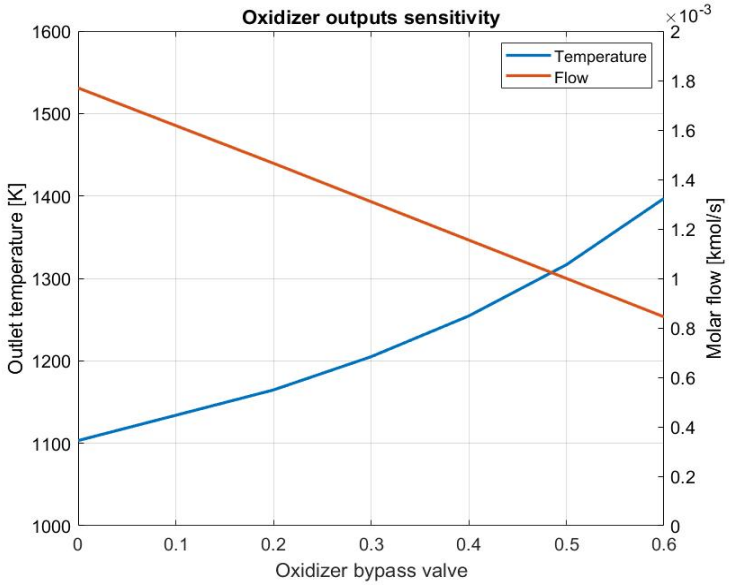


*Figure 10. Oxidizer bypass valve sensitivity. Design condition at 0.2.*

Thus, in order to find the optimal design condition, the two sensitivities have been combined, finding out if the main constraint for the heat exchangers downstream would have been the temperature (i.e. increasing the $\varphi$) or the total heat available (i.e. process more massflow, do not bypass air). The design condition showed also in the layout of Figure 6 , is with an HSU efficiency of 80% and oxidizer bypass of 20% of the total air flow form the outlet of the fuel cell.

# 3. Tri-generation fuel cell results

The dynamic hydrogen production depends on many variables of the system, especially the ones related to the solid oxide fuel cell. For this reason, before proceeding with the dynamic study of the system, an accurate understanding of the SOFC performance in steady state is required.

The inspiration of this work relies on the DEMOSOFC project and from the outstanding results proved in the OCSD tri-generation plant. Unfortunately, the actual data of the DEMOSOFC fuel cell were not available during the development of this study, so the data of a typical commercial industrial fuel cell have been used [29]. It means that the validation of the model has been done according to literature works, and not with the actual plant above mentioned. Although this could be a weak point of the work, that should be perfected whenever the data from the plant will be available, the author chose to perform a fairly thorough sensitivity analysis to explore which conditions lead to more benefits both in terms of fuel cell and system in general.

## 3.1. Sensitivity analysis

One of the information that fuel cell companies do not share easily is the flows patterns of the fuel and air streams, and in any case since the information is not available, the best choice consisted in analyze three main flows configurations: co-flow, counter-flow, cross-flow. The results from steady state simulations are in perfect agreement with literature [55], [60]: as shown in Figure 11, the co-flow configuration produces the maximum temperature drop because both air and fuel entering in the cell are at their lowest temperature, and because of the internal reforming, the temperature of the cell breaks down. Moreover, because of the huge initial drop, this configuration produces also the maximum temperature gradient across the entire cell (i.e. x direction) and the outlet streams are at the highest temperature, whereas the electrical performances are very low.

In the cross-flow configuration, although it has a better distribution of the reactants, the electrical efficiency is lower and the highly heterogeneous current distribution produce an important temperature gradient in the PEN layer, with

the maximum stress along the direction perpendicular to the fuel flow (i.e. y direction).

The counter-flow configuration presents the best performance, as expected. The air inside the cathode channels has the highest temperature where the heat for the internal reforming is required, producing an average temperature higher than the other cases and consequently the ohmic loss is smaller in the first part. Therefore, for this reason and for the fact that it requires less fuel flow with respect to the others, this configuration has the highest efficiency. Another consideration regards the outlet temperature of the oxidant flow, which is at least 20°C lower than the cross-flow and even more for the co-flow: it means that if the system layout can work in terms of heat recovery with that temperature, for sure it would work with higher outlet temperatures as well (i.e. precautionary conditions). In all three configurations, there is no appreciable difference in the hydrogen production, but still the counter-flow is the preferable one because the hydrogen molar fraction is the highest (Table 8).

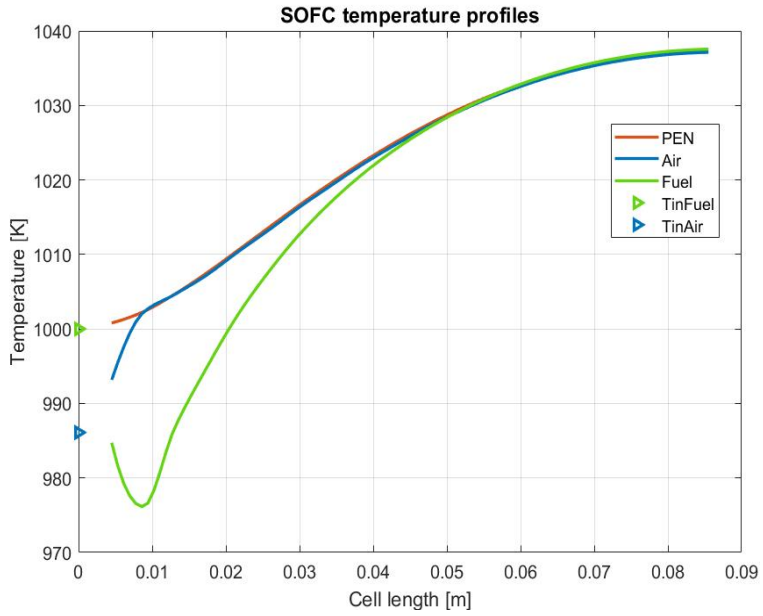


*Figure 11. Temperature profiles inside the fuel cell in co-flow configuration.*

| Parameter | Co-flow | Counter-flow | Cross-flow |
|---|---|---|---|
| V [V] | 0.816 | 0.819 | 0.817 |
| I [A] | 19.86 | 19.77 | 19.82 |
| TairOut [K] | 1038 | 1003 | 1024 |
| TfuelOut [K] | 1038 | 1034 | 1038 |
| AirFlow [kmol/s] | 1.76E-03 | 1.74E-03 | 1.75E-03 |
| TairIn [K] | 986 | 955 | 976 |
| FuelFlow [kmol/s] | 5.66E-04 | 5.64E-04 | 5.65E-04 |
| Exothermicity [$kW_{th}$] | 4.11 | 3.87 | 3.98 |
| $H_2$production [kmol/s] | 1.847E-04 | 1.844E-04 | 1.843E-04 |
| $H_2$fractionOut [-] | 21.72% | 21.78% | 21.72% |
| Efficiency [-] | 0.463 | 0.465 | 0.464 |
| MaxPEN [K] | 1037 | 1034 | 1038 |
| PENdeltaT [K] | 36.0 | 30.8 | 37.5 |
| StackdeltaT [K] | 51.7 | 47.0 | 48.3 |
| MaxdT/dx [K/cm] | 70.2 | 67.2 | 68.5 |

*Table 8. Comparison among three different flows configuration.*

In the Figure 12, the temperature distribution for the different configuration is provided to highlight the different position of the hotspots inside the cell: in the cross-flow configuration (top-left), the maximum temperature value of 765 °C is expected at the top-right corner of the cell, and the outlet of both air and fuel streams where the air is hotter and the electrochemical reaction is dominant. In the other two configuration the profiles are symmetric (therefore, the model can be run in a 1D domain) and in both the cases the hotter zone is at the exit of the fuel flow, because is the area where the stream is richer of hydrogen content.

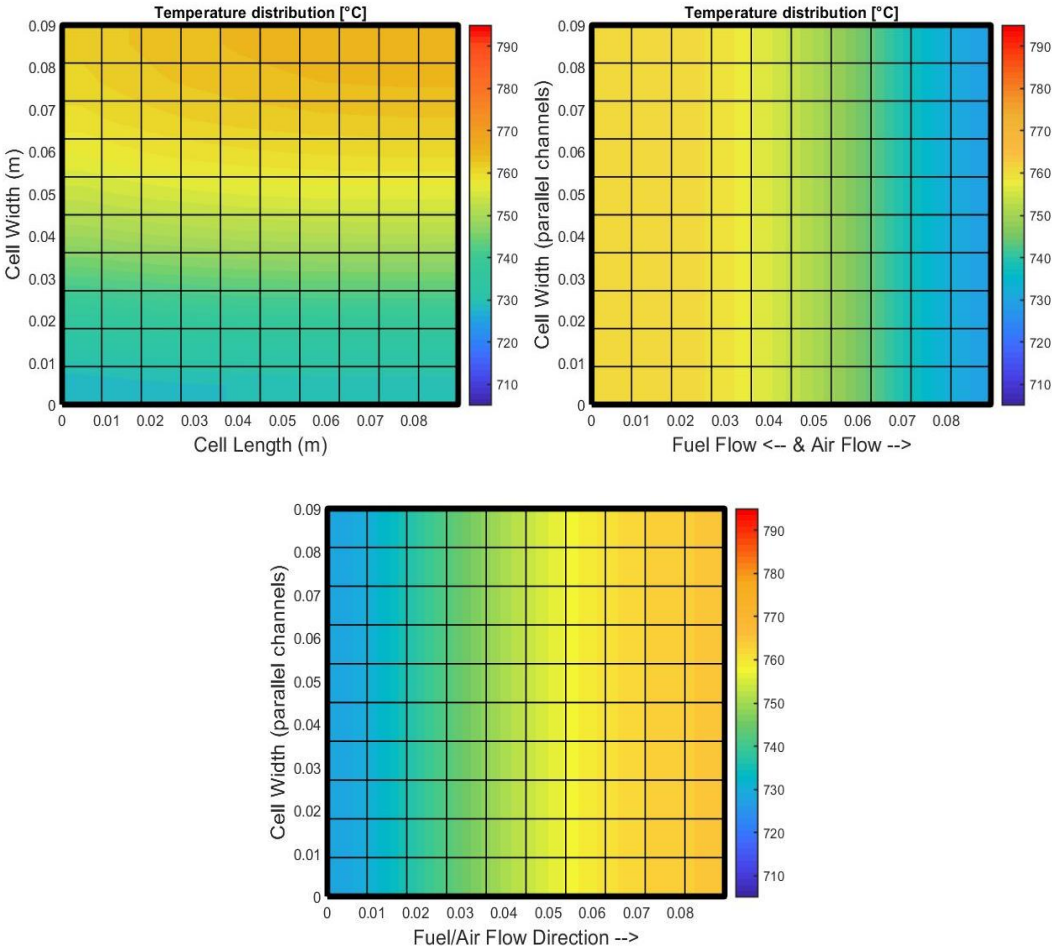


*Figure 12. PEN temperature distribution in cross-flow (top-left), counter-flow (top-right) and co-flow (bottom).*

Another important choice regards the Steam to Carbon ratio (S/C). The model does not include Boudouard equilibrium or methane cracking, but a proper quantity of steam should be mixed with the biogas in order to not have carbon deposition in the fuel cell. The choice of the S/C has to deal with performance and safety of the device: moving towards higher S/C (e.g. >2.5), the carbon deposition is basically avoided and the fuel cell can work in safe condition but the partial pressure of the active species which contribute to the Nernst potential decreases; moreover, with a S/C >2, the reaction rate of the SMR and WGS increases requiring more heat in the very first part of the cell. This extra need widens the temperature difference between the two extremities of the cell. On the other hand, using a poor mixture of steam and biogas (S/C <2), the risk of having solid carbon particles at the inlet of the fuel cell increases even though the voltage will be higher and the temperature a little bit more uniform due to the slower

reaction of methane along the channel [25]. At system level, producing a higher S/C flow requires more heat for the steam production. The yield of hydrogen production according to the S/C and temperature is already at the highest plateau as showed by previous work. [63]. Using a S/C =2, has proved to be an excellent trade-off, as several authors did in previous work [51], [64]. In the Figure 13 the spatial distribution of the S/C shows clearly how the ratio is always higher than 2, which is only the inlet value and also the zone with the higher risk of deposition.

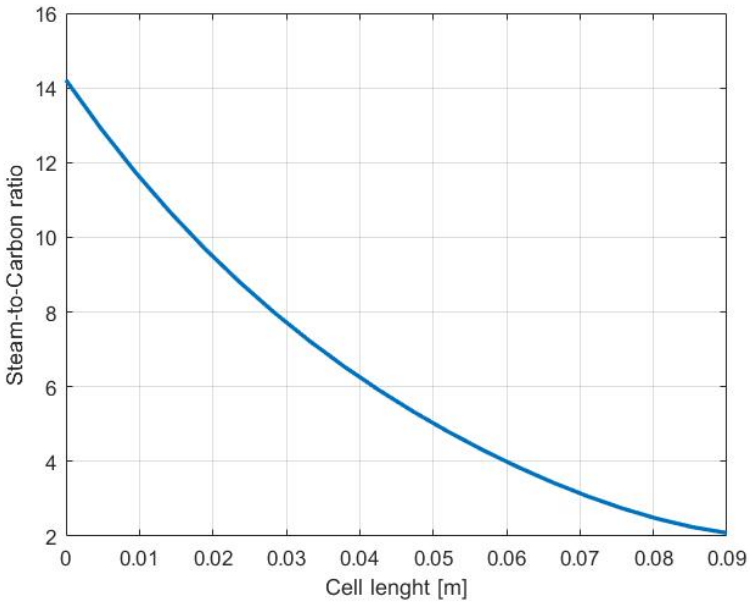


*Figure 13. Steam-to-carbon ration trend along the fuel cell domain.*

The analysis concerning the reformate supplied to the fuel cell has been already discussed in the previous chapter. As further support to the reformate choice (named Fuel 450 in the Table 5), the Figure 14 shows what happens in terms of temperature inside the PEN layer. As expected, the influence of SMR affects the temperature distribution in the PEN layer conveying to greater $\Delta T$ without any percentage of pre-reforming (i.e. biogas 65% CH4, 35% CO2) whereas in the case of Fuel600 that corresponds to 16% of CH4 reformation, the difference is reduced by 12 K from the former case. However, the advantages of choosing the Fuel450 instead of Fuel600 have already been explained in 2.4.3.

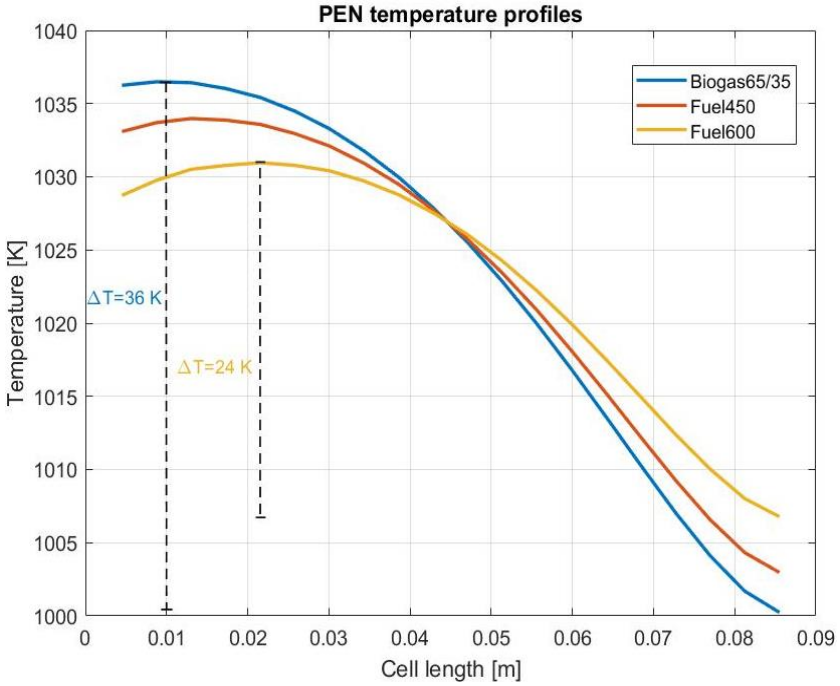


*Figure 14. PEN temperature profiles in counter-flow (design condition) with different fuel composition.*

Anyway, the previous choices do not influence the study of the thermoneutral point of the fuel cell as much as the utilization factor does. In this sensitivity analysis, the first goal was to figure out in which condition the fuel cell started to behave as endothermic device, and the results are presented in Figure 15. Thermoneutral point for different PEN average temperatures are provided in function of the average temperature. For example, the exothermicity of the cell is supposed to increase of about 10 times when the cell operates at 973 K instead of 1123 K at the same fuel utilization factor.

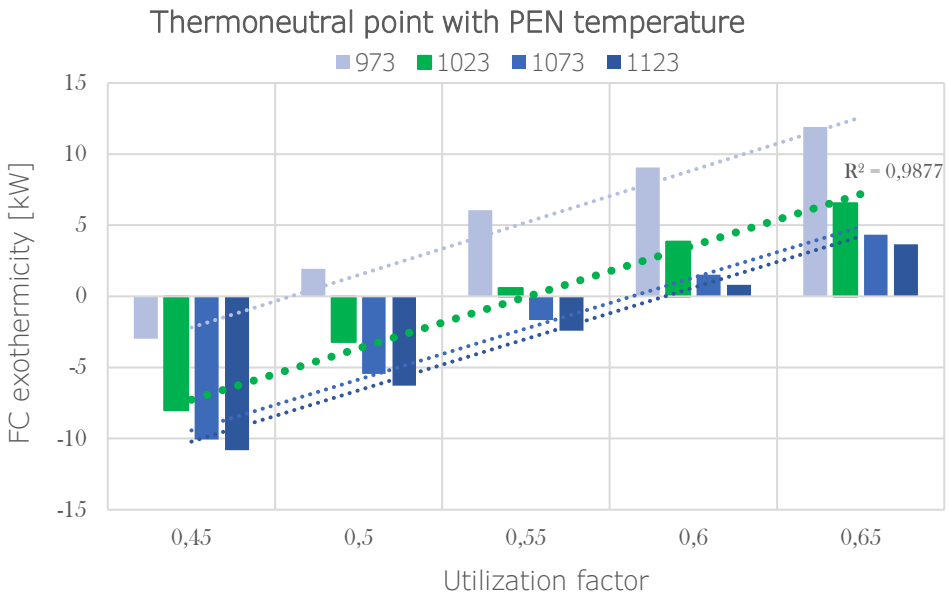


*Figure 15. Thermoneutral point for different PEN average temperatures*

The reason of this "shifting thermoneutral" according to the temperature comes from difference in the SMR load. For example, at higher temperature the endothermic reaction of reforming is favored and at the same utilization factor of the fuel the heat absorbed is higher. The thermoneutral point on the utilization factor domain, is moving towards higher percentage when the average temperature increases also because in the balance of the exothermicity, the contribution associated with the irreversibilities of the cell decreases because the cell performs better at higher temperature. For this reason, the thermoneutral condition in the case of 1023 K is around $U_f \approx 0.55$. Other than this proof of endothermicity dependence, the important variables evaluated for the choice of the design condition are listed in Table 9, and in the last column the direction of the arrow indicates in which way the utilization factor has to change to get better values.

| Parameter | Reason | $U_f$ |
|---|---|---|
| Air Inlet Temperature | Heat load | ↑ |
| **Air Flow** | Electrical load | * ↓ |
| Temperature gradient | Thermal stresses | ↑ |
| Fuel yield for $H_2$ production | Tri-generation | ↓ |
| Voltage | Electrical efficiency | ↓ |

*Table 9. Parameters of interest in the fuel utilization choice.*

The exothermicity of the cell is the fundamental marker to understand those optimal trends. For example, increasing the $U_f$ clearly increases the exothermicity of the cell and it means that the inlet temperature required for the air is lower. Moreover, still at higher utilization factor, the thermal stresses are reduced since the temperature gradient is less sharp because there is not a net difference between the zones in which the endothermic and electrochemical reaction dominate. This smoother profile of the temperature distribution is shown in Figure 16.

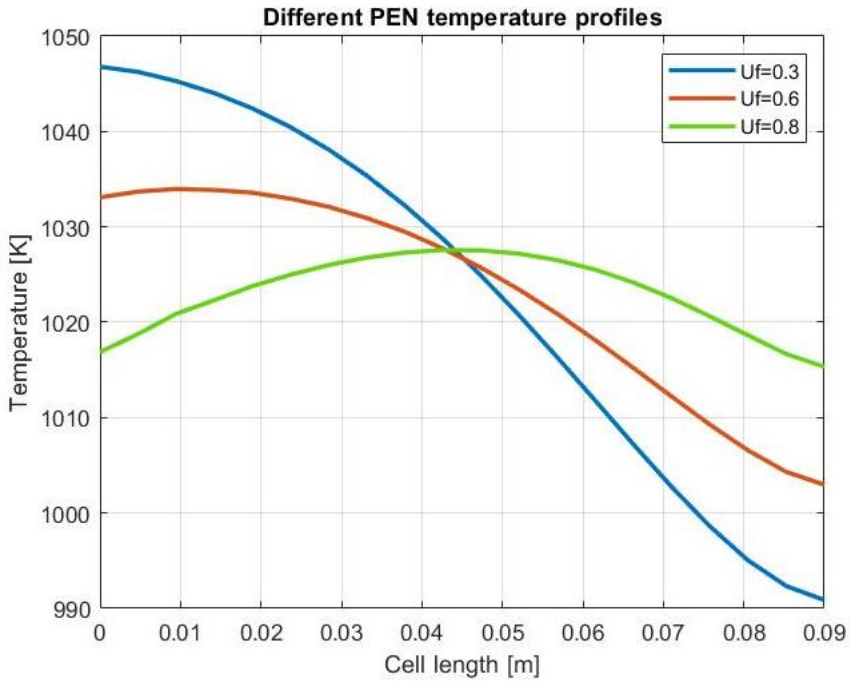


*Figure 16. Strong relationship of the PEN temperature profiles with respect to the utilization factor.*

Indeed, the increasing amount of heat needed for SMR because of greater fuel flow processed through the fuel cell combined with the less heat produced by electrochemical reaction since lower utilization factor, lead to an endothermicity condition of the cell below $U_f = 0.6$, whose trend is not linear.

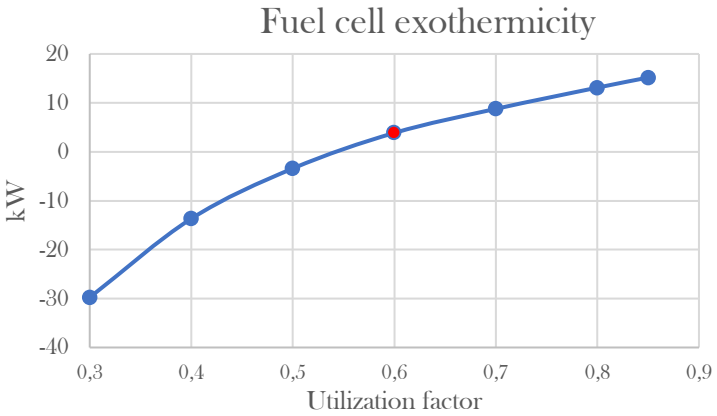


In any case, thanks to the winning control strategy of having a temperature difference set point across the stack, the maximum $dT/dx$ appears to be always below the SECA target of the DoE for SOFC (i.e. $10°C/cm$) [50]. Indeed, since the controlled variable is the $\Delta T_{stack}$, if that value is below the limit (e.g. 90°C as maximum for the mentioned cell 9x9 cm in the highest fuel utilization), the $\Delta T_{PEN}$ is definitely smaller than the stack value. Only in the 0.3 case, the gradient exceeds the recommendation limit. However, from Figure 17 it is clear how the entire profile of the cell becomes smoother if the SOFC works at higher $U_f$ because both the maximum thermal gradient and local temperature decrease.

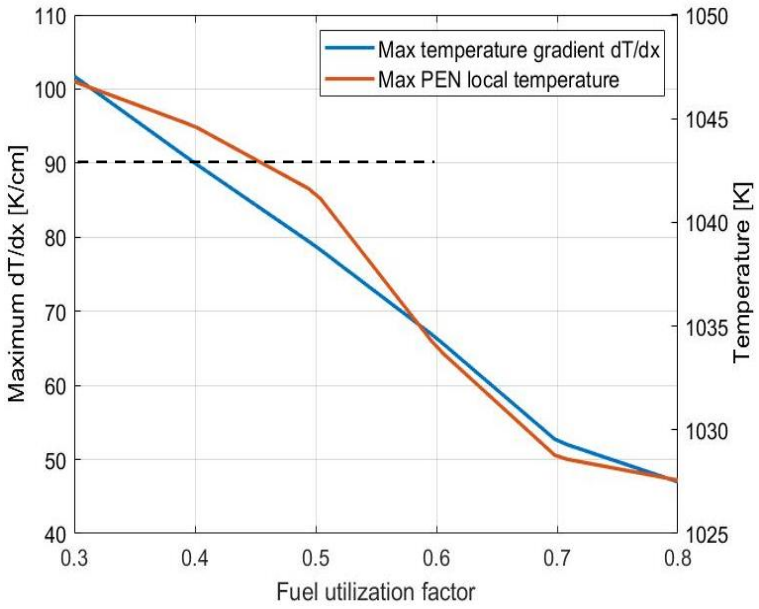


*Figure 17. Maximum local temperature gradient and PEN hot spot, at different utilization.*

Regarding the advantages of going down with the utilization factor, a trivial perk is for sure the increase of voltage due to higher fuel concentration along the cell, especially at the exit, increasing the Nernst voltage. The other evident reason is the hydrogen production, one of the goals of this work for tri-generation purpose. However, the interesting result is that the ratio between the hydrogen production and the reformate supplied presents a linear behavior, as shown in Figure 18, so the yield of hydrogen production increase undoubtedly. The linear trend is the direct consequence of the fact that both the hydrogen production in terms of molar flow follows the same trend of the fuel input. Moreover, the blue boxes in the same figure show the percentage of hydrogen content at the exit of the SOFC: the advantage of going down with the $U_f$ relies also on this aspect because it means that the partial pressure of the hydrogen will be higher at the inlet of the HSU affecting positively the operation of the PSA.

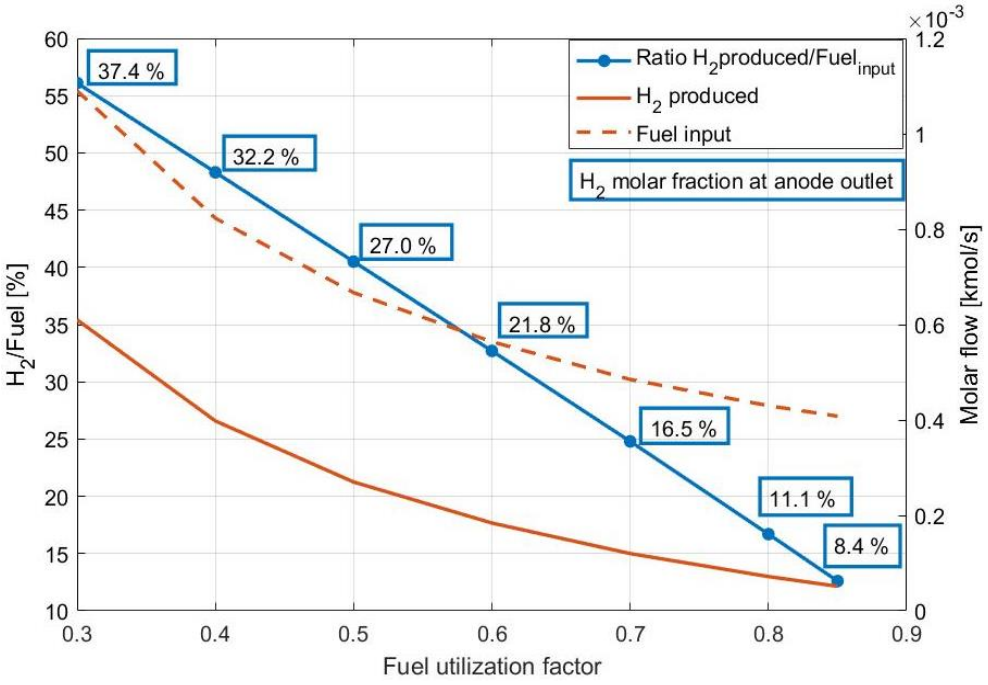


*Figure 18. Hydrogen production and molar fraction at SOFC anode outlet.*

In the air flow trend in Table 9, and asterisk is present because its trend presents a minimum:

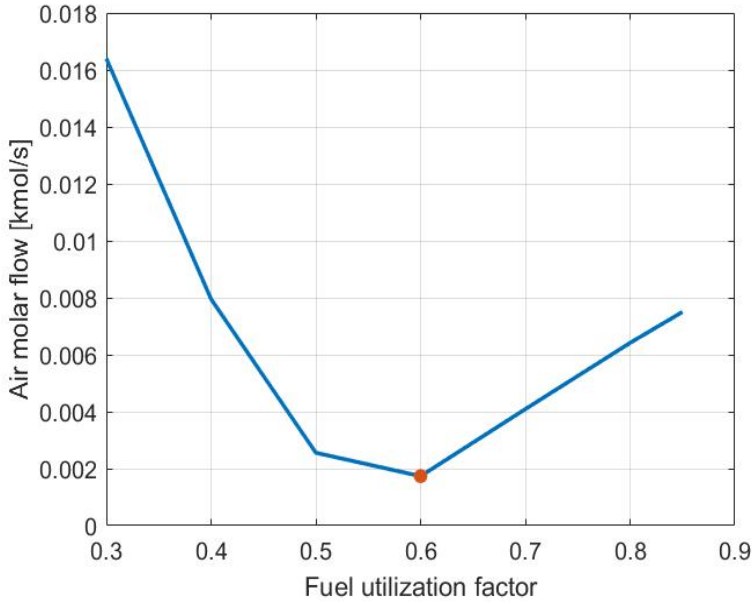


*Figure 19. Air flow result from utilization factor sensitivity*

This is an important yardstick to assess the performance around the net zero exothermicity condition: at higher factors, the exothermicity of the cell requires more air flow in order to cool down its temperature and to maintain a proper temperature difference across the stack; on the contrary with factors lower than 0.5, the cell needs a source to supply enough heat for sustaining the SMR and to reach the setpoint temperature, so the airflow will increase in that case but working as a source of heat.

## 3.2. Design condition results

The previous results from the sensitivity analysis (and from engineering assumptions) allowed the definition of the SOFC design condition, summarized in Table 10 in terms of model inputs, and as outputs in Figure 20.

| Parameter | Value | Units |
|---|---|---|
| Geometry | Counter-flow | - |
| Utilization factor | 0.6 | - |
| Fuel inlet temperature | 1000 | K |
| Fuel composition | Fuel450 | Table 5 |
| Air composition | 79% $N_2$ - 21% $O_2$ | - |
| Steam-to-carbon | 2 | - |
| Nominal power | 58 | kW |
| Current density | 0.25 | A/cm$^2$ |
| PEN avg temperature | 1023 | K |
| Stack $\Delta T$ limit | 60 | K |

*Table 10. Model inputs in the tri-generation design condition.*

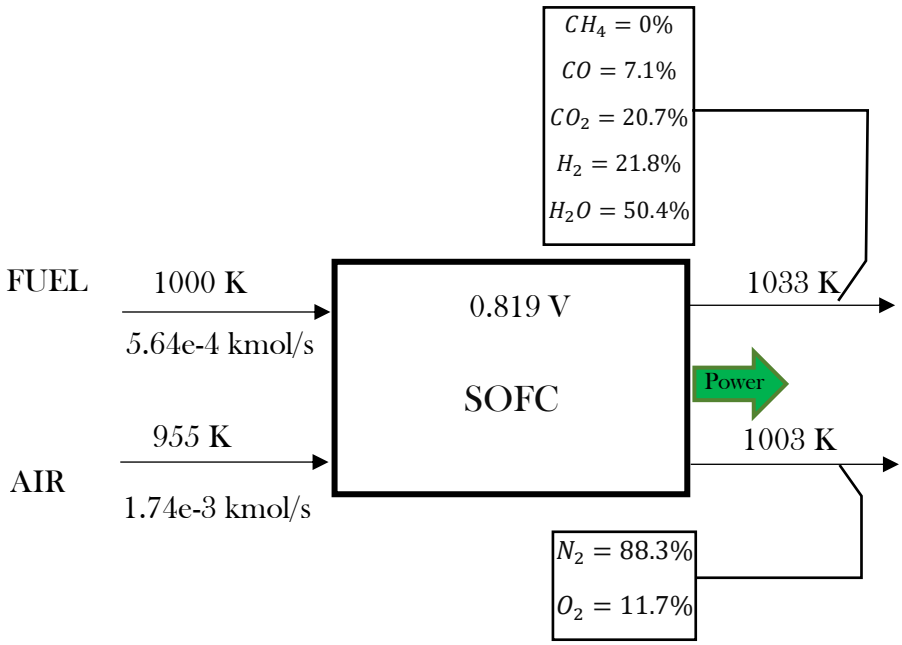


*Figure 20. Fuel cell inlets and outlets in design condition*

## 3.3. Validation

As previously mentioned, the EAGERS code has been validated many times along the years of its development. In any case, a small validation with Campanari's study has been done by the author. The comparison in terms of electrical outputs

(voltage and power) is provided for different configurations in Table 11, with the relative error of the current study for each variable in *italic*:

| Configuration | Variable | Achenbach [55] | | Campanari [56] | | Current study |
|---|---|---|---|---|---|---|
| Co-flow | V [V] | 0.6740 | *0.0%* | 0.6743 | *0.1%* | **0.6737** |
| | P [W] | 20.21 | *0.1%* | 20.24 | *0.0%* | **20.24** |
| Counter-flow | V [V] | 0.7080 | *1.0%* | 0.6930 | *1.2%* | **0.7010** |
| | P [W] | 21.23 | *2.0%* | 20.80 | *0.0%* | **20.8** |
| Cross-flow | V [V] | 0.6820 | *0.1%* | 0.6817 | *0.1%* | **0.6824** |
| | P [W] | 20.46 | *0.0%* | 20.45 | *0.0%* | *20.45* |

*Table 11. Validation results. Comparison with Achenbach experiment and Campanari's model.*

The maximum error in terms of voltage occurred in the counter-flow configuration, but it is around 1% compared with the Achenbach experiment. The outlet air temperature is also compared but omitted for brevity.

A further calibration of the model with the actual data of the Convion® fuel cell installed in DEMOSOFC project is highly recommended when they will be available because a specific validation with the plant in the co-generation mode and then in tri-generation operation would ensure the exact differences of performance of the same device.

# 4. System Results

Moving to system level, the simulations show more than just fuel cell performance, although its outputs must be the same of the steady state design condition presented in chapter 3. In order to understand the behavior of the system when moving from a tri-generation design condition to co-generation mode, increasing the fuel utilization, other components previously introduced have been included.

The main focus in this chapter consists in describing how the fuel cell reacts to a change in its electrochemical behavior (e.g. utilization factor) and power load, taking into account the dynamic of the heat exchangers, blower and valves.

## 4.1. Off-design steady state

The first dynamic study regards the change in fuel utilization in order to shift the main goal of the plant from hydrogen production to a cogeneration plant delivering only power and heat. The assumption hereby was to keep constant the electrical output of the fuel cell at the rated power, in order to highlight the difference in fuel consumption to produce hydrogen as third product. Therefore, the change in fuel utilization from 0.6 to 0.85 when moving from tri-generation operation to co-generation, has a direct impact on the fuel flow required by the cell (as input) and on the hydrogen production at the anode outlet (as output).

The design condition has already been presented in Figure 6 and before showing how the system reacts during the transient, the new steady state condition at fuel utilization of 0.85 is illustrated in Figure 21.

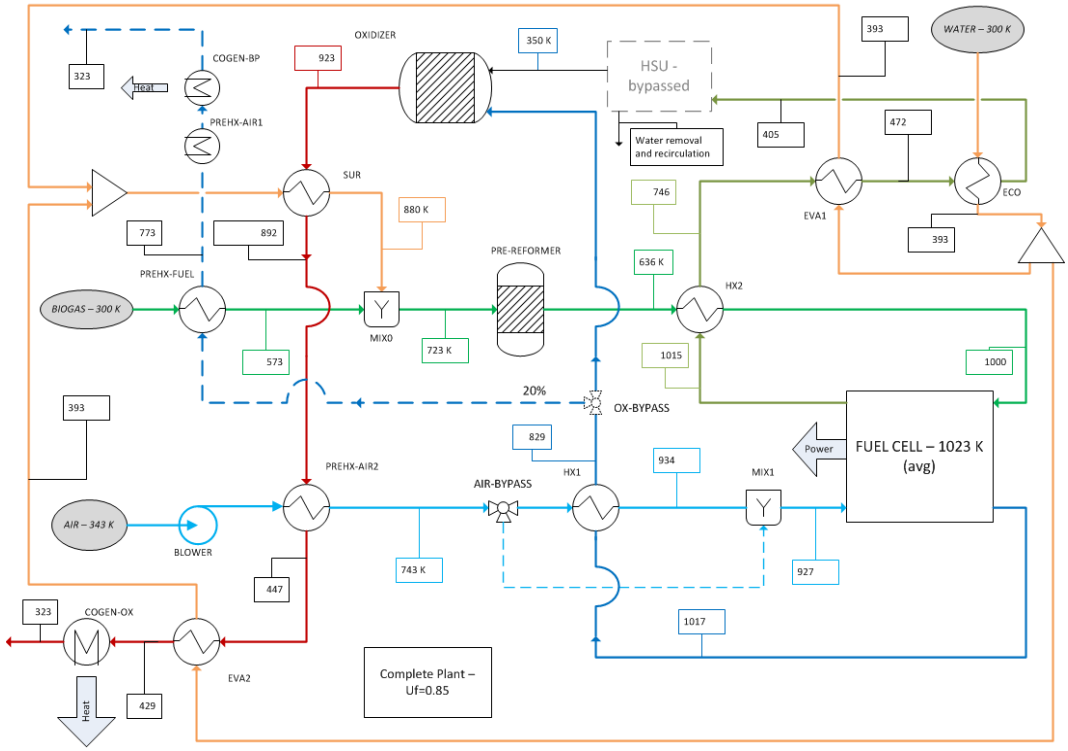


*Figure 21. System layout in off-design condition: utilization factor at 0.85, cogeneration system only.*

Three main differences are pointed out in the following figure, where the simplified version of the dynamic simulation is provided: when the hydrogen production is not required, the plant can shift its operation producing the same rated power, but having more heat available for cogeneration due to the bypass of the HSU (and the air flow sent to the oxidizer is also bigger, as shown in Figure 19). Quantitatively, this new off-design steady state can produce +38% of heat available at 923 K, which is still suitable for warming up the incoming streams and the net co-generation for the WWTP requirements while the fuel consumption (supplied to the SOFC) reduces of almost 40%. Then, as discussed in chapter 3, when operating at $U_f = 0.85$ the SOFC becomes more exothermic, and according to the control strategy adopted to keep constant the PEN temperature and do not exceed the limit for the $\Delta T$ of the cell, more air flow (and colder) will be sent through the cathode side and it means that a bigger mass flow of depleted air will react in the oxidizer with the residual from the anode outlet after water condensation. The air flow is used to control the $\Delta T_{stack}$ whereas the inlet temperature should regulate the $T_{PEN}$: when the mass flow increases because the outlet of the fuel cell becomes hotter, the blower power increases in order to

supply more air and the temperature at the exit of the HX1 changes. At this point, if the inlet temperature of the fuel cell is still too hot, the bypass valve will mix a colder air before entering in the cathode side. This is an important action of the valve especially during the transient as shown later in 4.2, because if the inlet conditions in terms of flow and temperature do not follow quickly the new conditions inside the cell, the cell could behave very far from the set point values. Moreover, the faster dynamic of the valve with respect to the blower, allow the controller to open and close the valve following the rapid change in temperature of the cell. Although during this particular transient (moving from 0.6 to 0.85 utilization) the valve opens until almost 40%, when the new steady state condition is reached, the total mass bypassed is 3.8% without wasting too much energy in the mixing, and the inlet temperature decreases by 27 °C compared with the design case. In this case another sensitivity analysis on the percentage of the oxidizer bypass has been carried out and the results showed that keeping it constant at 20% as in the tri-generation case would be the best choice to allow the heat recovery downstream.

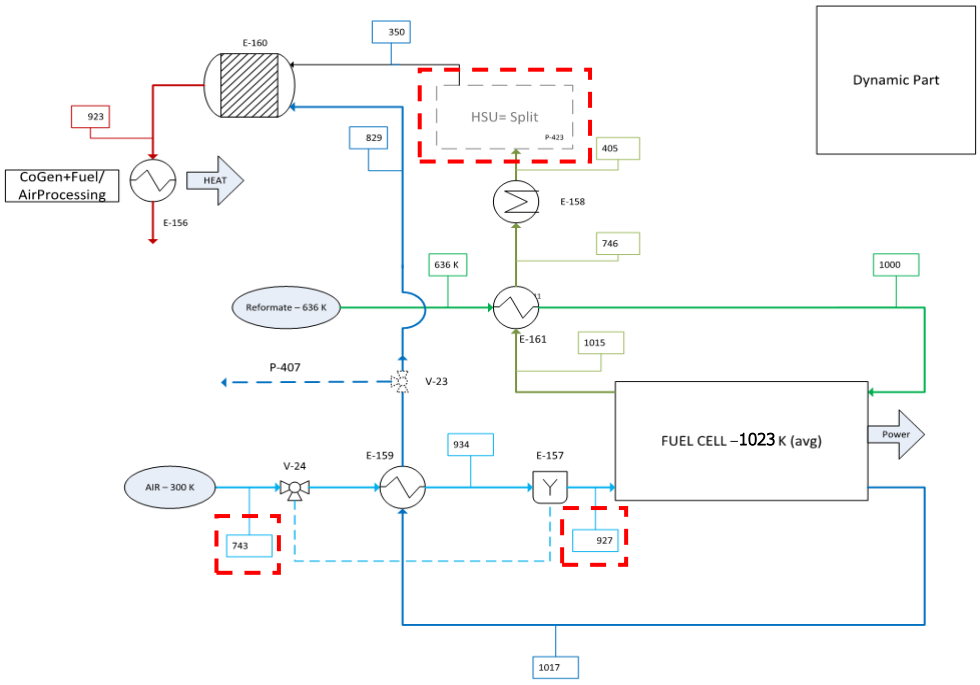


*Figure 22. Dynamic layout at Uf=0.85.*

In Table 12, the main difference between the two distant conditions for which the plant has been considered are summarized. The maximum heat available means the maximum quantity that can be recovered for the net co-generation and the HSU recovery percentage stays for the percentage of hydrogen that can be separated with respect to the inlet stream in the HSU block.

| Parameter | Tri-generation mode | Co-generation mode |
|---|---|---|
| Utilization factor | 0.60 | 0.85 |
| Voltage [V] | 0.819 | 0.802 |
| Current [I] | 19.78 | 20.19 |
| Fuel flow [kmol/s] | 5.64e-04 | 4.06e-4 |
| Air flow [kmol/s] | 1.74e-03 | 4.93e-03 |
| $H_2$ at anode outlet [kmol/s] | 1.85e-04 | 5.12e-05 |
| Blower consumption [kW] | 1.85 | 2.95 |
| $Heat^{MAX}$ available [kW] | 14.1 | 19.5 |
| Air bypass [%] | 0 | 3.8 |
| SOFC electrical efficiency [%] | 46.5 | 64.6 |
| HSU recovery [%] | 80 | 0 |

*Table 12. Difference between tri-gen and co-gen operation at steady state: values refer to each module of 58 kW.*

In this new off-design condition, the distribution of the reactant inside the fuel cell changes a lot as shown in Figure 23, and with them the SMR, WGS and electrochemical reaction, leading to a new temperature distribution inside the cell.

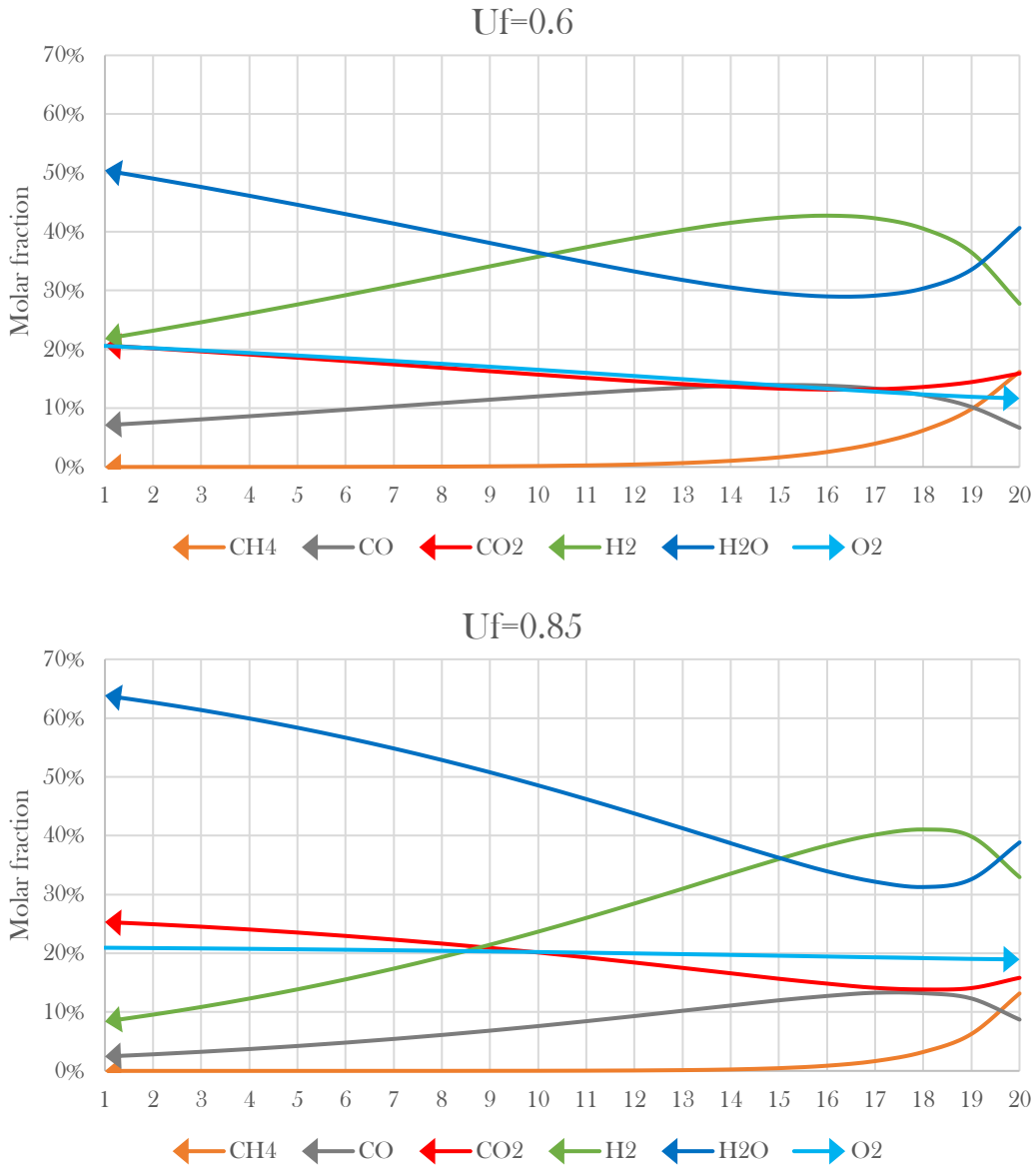


*Figure 23. Species concentration along the cell. Molar fraction in each node of the space discretization.*

The change in the outlet concentrations is quite relevant because the hydrogen molar fraction drops down to almost 8% (more than 63% of the mixture is made by steam) at the highest utilization factor.

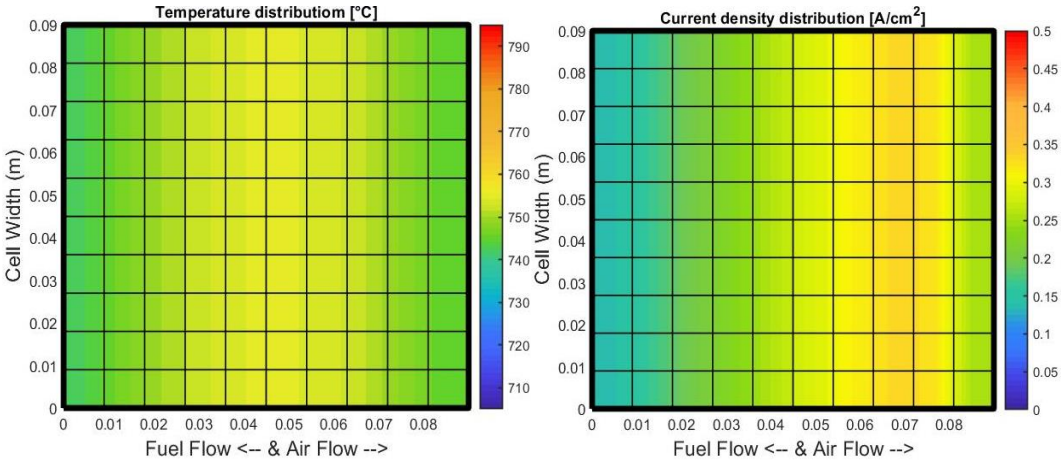


*Figure 24. Temperature and current density distributions at new steady state condition of Uf=0.85.*

In Figure 24, the temperature distribution inside the PEN layer is in perfect agreement with what showed in the previous sensitivity study, because the profile is smoother along the cell. The maximum temperature appears to be in the middle of the cell instead of the exit of the fuel as in the 0.6 case: the reason relies on the hydrogen distribution, which is different and after 2/3 of the cell length is almost depleted. The same reason is responsible of the current density distribution on the right of the same figure. Indeed, the peak in hydrogen concentration occurs around 0.07 m (in the picture) that is about 1/3 from the fuel inlet, and in that are both Nernst voltage and current density are higher, since the equipotential constraint of the voltage must be respected.

Regarding the second dynamic, in terms of power adjustment, the most interesting result regards the increase of power above the nominal value. There are two main reasons. First, this study has been thought to be useful mainly for tri-generation concept in WWTP, and according to literature the power consumption of the plant is always higher than the power that can be produced only by the biogas which is produced by the plant itself [62], so the electricity production through the fuel cell modules can cover only part of the total load. Hence, there is actually no need to reduce the electrical output on purpose. Second, the goals with which this plant has been designed are the hydrogen production coupled with power and heat available for the plant itself, going out of the plant with one useful product intended for other users. In order to optimize the heat recovery of the system and having a net cogeneration for the sludge heating, the system as described does not

foresee an operation with the fuel cell that has an average temperature below the set point imposed, which is one of the consequences when the power output reduces. However, since the fuel input follows directly the power load and the hydrogen production is strongly related to the fuel processed through the SOFC, a second regulation of the hydrogen production via power changes is possible because without altering the electrochemical condition inside the cell the hydrogen flow can be increased or decreased together with the electricity production.

| Power | 70% | 100% | 120% |
|---|---|---|---|
| Exothermicity [kW] | 2.2 | 3.9 | 7.1 |
| Current density [A/cm2] | 0.17 | 0.24 | 0.30 |
| FuelFlow [kmol/s] | 3.88e-04 | 5.64e-04 | 6.98e-04 |
| Hydrogen production [kmol/s] | 1.31e-04 | 1.84e-04 | 2.28e-04 |
| PENdeltaT [K] | 20.2 | 30.8 | 33.2 |

*Table 13. Main parameters of the SOFC at different power loads.*

However, few simulations with power step and sinusoidal changes are presented in Figure 25 and Figure 26 to show the response of the fuel cell in terms of average temperature, thermal stresses, and hydrogen production in the design condition. When the power is below the nominal value, the amount of fuel (and the corresponding air) needed is smaller: in order to keep constant the average temperature, the fuel flow and air flow must reduce to stabilize the cell upon new condition at 40 kW. In this simulation the PEN average temperature decreases until 980K because of the minimum air flow constraint imposed. The minimum air flow was imposed in a first moment to ensure enough air (i.e. air utilization) for the electrochemical reaction, and the following plots have been chosen to explain the impossibility to increase only the air temperature with the current layout. Instead, when the fuel cell works above the nominal power, for example at 70kW, the working point moves towards higher current density (the exothermicity of the SOFC increases as well) and the temperature of the cell would naturally rise while the controller is able to keep the average temperature at 1023 K.

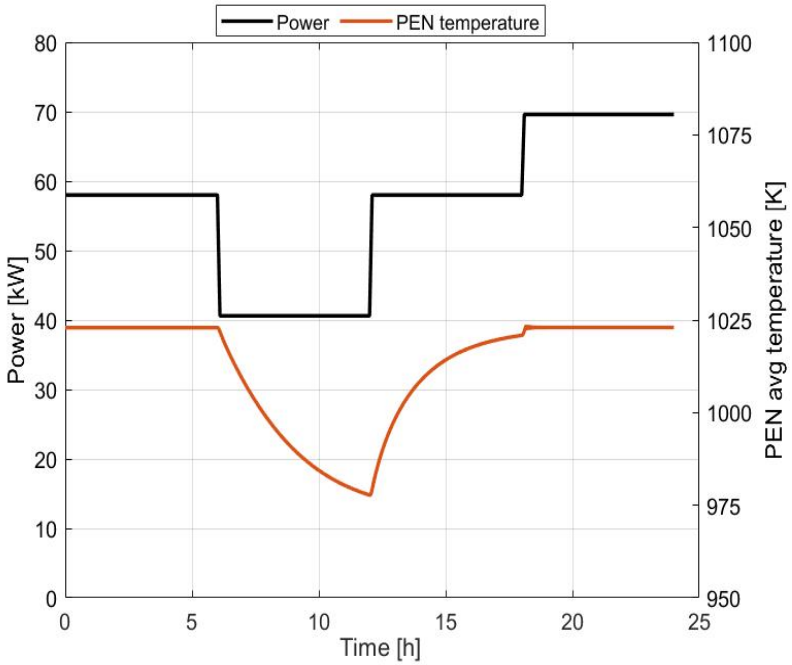


*Figure 25. Power step changes: 100%, 70%, 100%, 120% for 6 hours each.*

An interesting take away from the sinusoidal input profile, is the different dynamic that occurs at electrochemical and thermal level. When a sinusoidal power input is imposed with an amplitude of ± 20% with respect to the nominal power over a period of one day (24h), the thermal dynamic of the SOFC is slower than the response of the cell in terms of electrochemical parameters (which follow perfectly the power input): for example, the cell reaches its minimum temperature after 70 minutes compared to the minimum power.

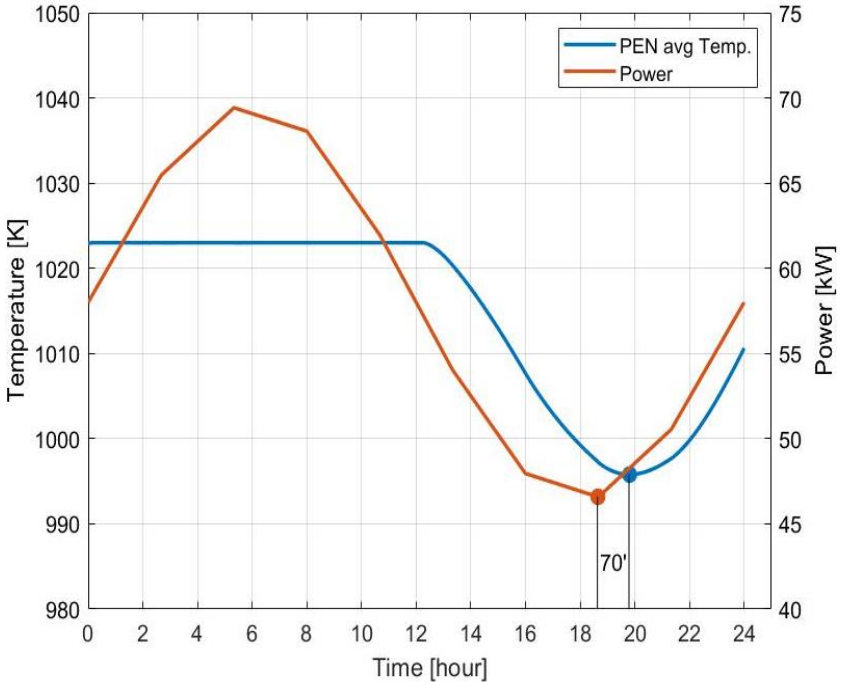


*Figure 26. Power with sinusoidal profile. Different behavior in terms of temperature when above nominal power and when below nominal value.*

## 4.2. Dynamic simulations

In this section more details are provided to explain deeper what happens during the transient. First, the dynamic that involves the power showed an important result that could not be seen in the steady state simulations about the interconnector thickness. To explain the importance of the IC thickness, two simulations with different thickness are provided in the following plot.

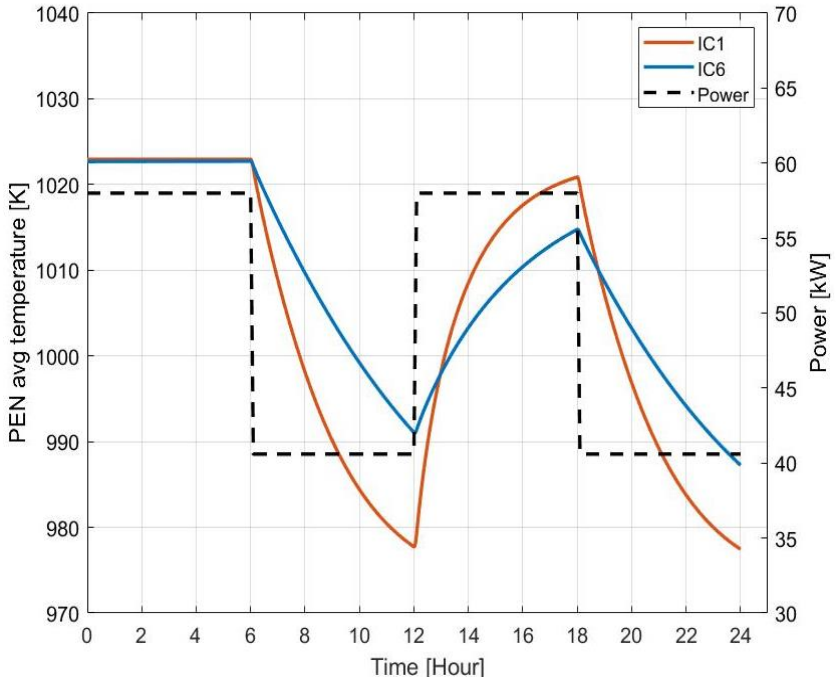


*Figure 27. Interconnector importance in the dynamic operation.*

Looking at the red curve in Figure 27 (IC1 represents the IC of the reference cell of the work), giving as input a variable load of 100% and 70% of the nominal power (with the minimum oxidant flow value), the cell temperature breaks down because the operating point is moving towards lower current densities and the exothermicity of the cell is reducing. If there is not possibility to increase the inlet temperature of the air and of the fuel with the current design, the cell cannot sustain its set point temperature without external input. In this plot, it is clear how the thermal mass of the fuel cell plays and important role. With a thicker interconnector (blue curve, thickness of 6mm) , the fuel cell can maintain a higher temperature for a longer period since the thermal dynamic is slower. In 6 hours at 70%, the default fuel cell used in the study explored a temperature drop of 45 K which means decreasing its average temperature of 7.5 K per hour. If the same fuel cell with an IC thickness of 6mm (e.g. other companies have used thicker IC [51]) was used, the $dT_{PEN}/dt$ would have been of about 5 K per hour. This is an important result because the choice of the interconnector that makes up most of the weight of the cell should be considered in the design according to the conditions in which the system is going to work. A thinner IC could reach sooner a new steady condition, but the fuel cell would face tougher conditions in terms

of thermal cycle and electrochemical stability. On the other hand, with an IC of several mm, the temperature drop will be attenuated and especially for short transients (few hours), the temperature can be maintained also in this configuration.

However, with the IC parameter chosen for the SOFC of the study, an example of step changes in power from the 100% to the 120% is provided together with the change in hydrogen production and the exhaust conditions from the oxidizer in Figure 28.

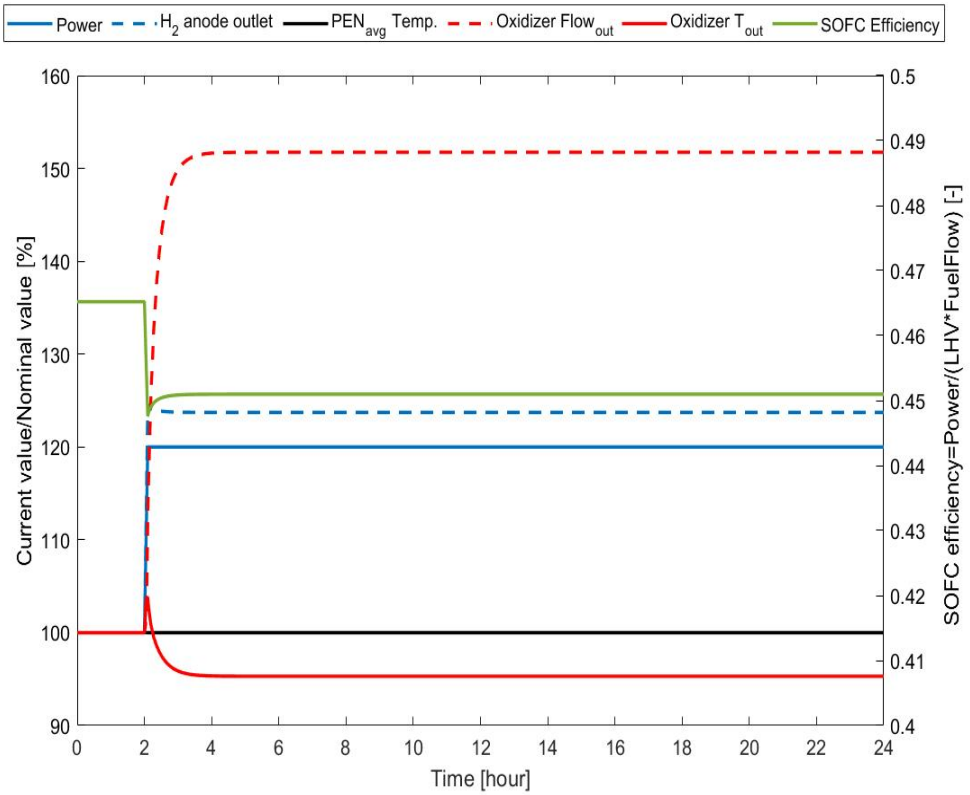


*Figure 28. Response of the tri-generation plant to a power increase of 20%.*

Besides the temperature trend that is constant during the whole transient, two important information come from the previous plots regarding the two co-products which are strongly related to the power production. The change in power implies a change in fuel flow at constant utilization factor, so the hydrogen production will scale with the fuel flow and in this specific case will increase. In the same moment the available heat downstream of the oxidizer changes because the inlets of the oxidizer are changing as well: the outlet temperature decreases

because the equivalence ratio is smaller, but the total mass flow of the exhaust increases since the fuel and air flows are bigger than the nominal condition. Therefore, a reduction of the power can be seen as a reduction of all the three products of the plant whereas the operation above the nominal power can be seen as increase of the co-products. However, this last comment should not be seen as a limitation of the system because it allows the plant to reduce or raise the production of the $H_2$ without involving the change in the electrochemical behavior of the cell through the utilization factor. For instance, if the hydrogen production needs a quick increase or decrease, the regulation through the power is preferable with respect to the fuel utilization because has a longer dynamic. Unfortunately, the SOFC efficiency decreases since the cell works at higher current density explaining the increase of the cooling load because the irreversibility (i.e. exothermicity) of the cell is more important. This scenario opens another further study about the economic value of those products: if the economic value of the hydrogen production is higher than the value of the electrical energy produced by the SOFC, it is possible to shift the focus on the hydrogen production only and optimizing the use of the biogas according to the hydrogen demand, adjusting the fuel cell working condition considering only the economic value of the hydrogen as a product.

The second dynamic investigates the response of the system when the utilization factor changes, ensuring that the controller strategy will be able to keep constant the set points of the cell, and this study needs to demonstrate the safe condition of the cell during the transient. The Figure 29 is interesting because it allows the plant to move from a design condition in which the additional production of hydrogen as third product is sought to the more conventional operation at higher fuel utilization. As first result, the electrochemical dynamic is faster than the thermal induced dynamic (e.g. the average PEN temperature) and this is perfectly in agreement with literature [59] and previous results. The step change in the $U_f$ can be quite sharp, but the control system reacts very well in order to keep the temperature constant when the fuel factor increases because the air bypass valve ensures a proper inlet temperature. When the fuel cell returns to work at 0.6, a temperature drop is verified for few hours because the air flow is also changing to

control the temperature difference across the cell whereas the bypass is already closed, but they have a different quickness.

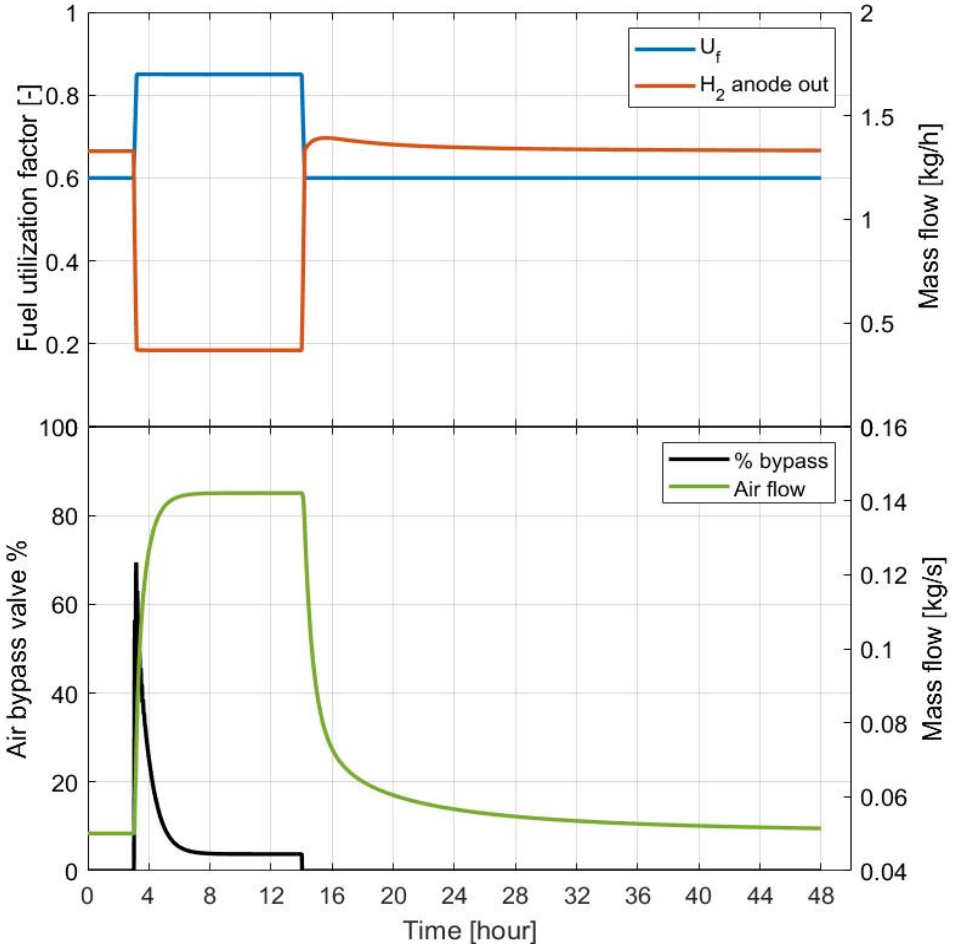


*Figure 29 Fuel utilization change: (top) sharp variation of the utilization factor leads a quick change in hydrogen availability at the anode outlet; (bottom) controller variables to keep the PEN temperature constant and contain the $\Delta T$ across the cell.*

The HX1 has also its dynamics that influence the outlet temperature of the fresh air. The dynamic is not so fast because of the change in the mass flows through the HX and because the heat exchanger has its own thermal capacity mainly due to the solid layer.

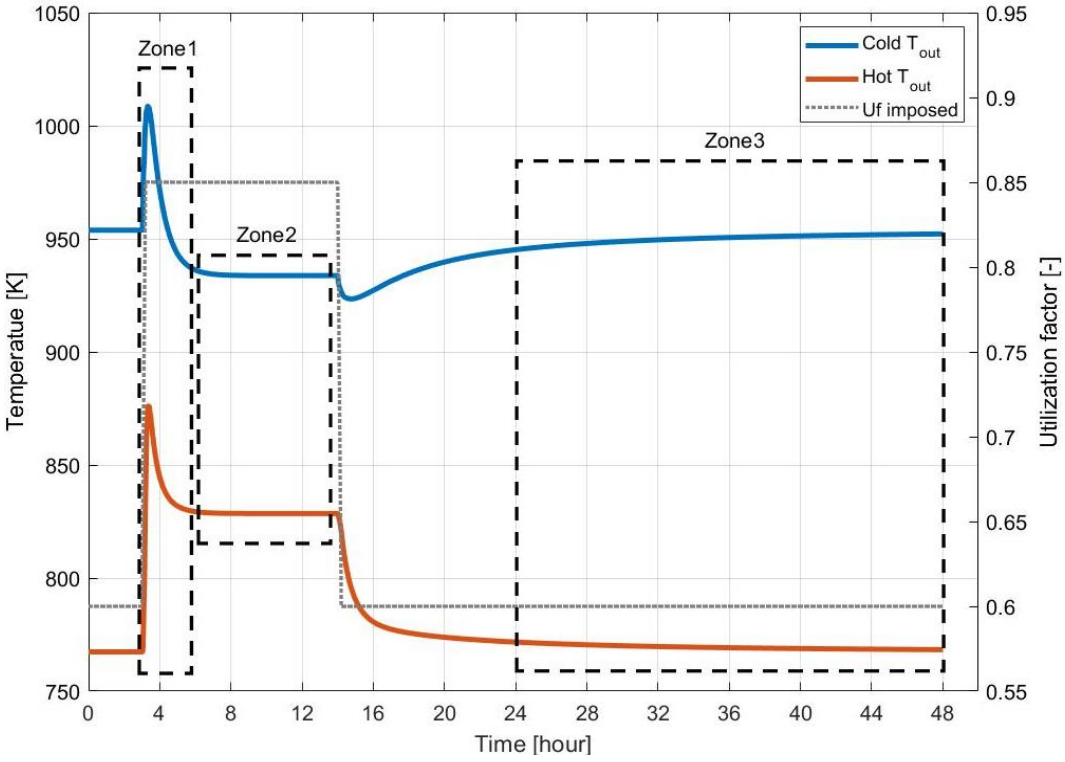


*Figure 30. Air heat exchanger outlet temperatures during the dynamic of Uf (HX1).*

Three main zones can be individuated in the Figure 30 representing the outlet temperature of the cold flow (i.e. fresh air) and the hot flow (i.e. cathode outlet):

1. Zone1 is characterized by strong instability in the heat exchanger because the outlets of the SOFC are changing because of the change in the utilization factor, and the air flow is changing as well because the controller is acting to maintain the set points. The quick increase in temperature depends on the higher outlet temperature from the fuel cell, due to the higher exothermicity, as shown in the general layout (the cathode outlet temperature passes from 1003 K at 0.6 to 1017 at 0.85). Moreover, the air bypass valve opens as soon the temperature of the PEN would start to increase, and a smaller air flow passes through the HX1.
2. Zone2 represents the new steady state condition at $U_f = 0.85$. After 2 hours from the fuel utilization perturbations, the air flow and temperature are stable, and the plant works as previously illustrated in Figure 21.
3. Later, when the utilization factor goes back to 0.6, another small perturbation is explored until the Zone3, where the initial steady state conditions are reached.

Another important result consists in the fact that when the fuel cell works at higher fuel utilization the temperature profiles is completely different from the lower factor condition, and its trend contains the temperature gradient (Figure 31).

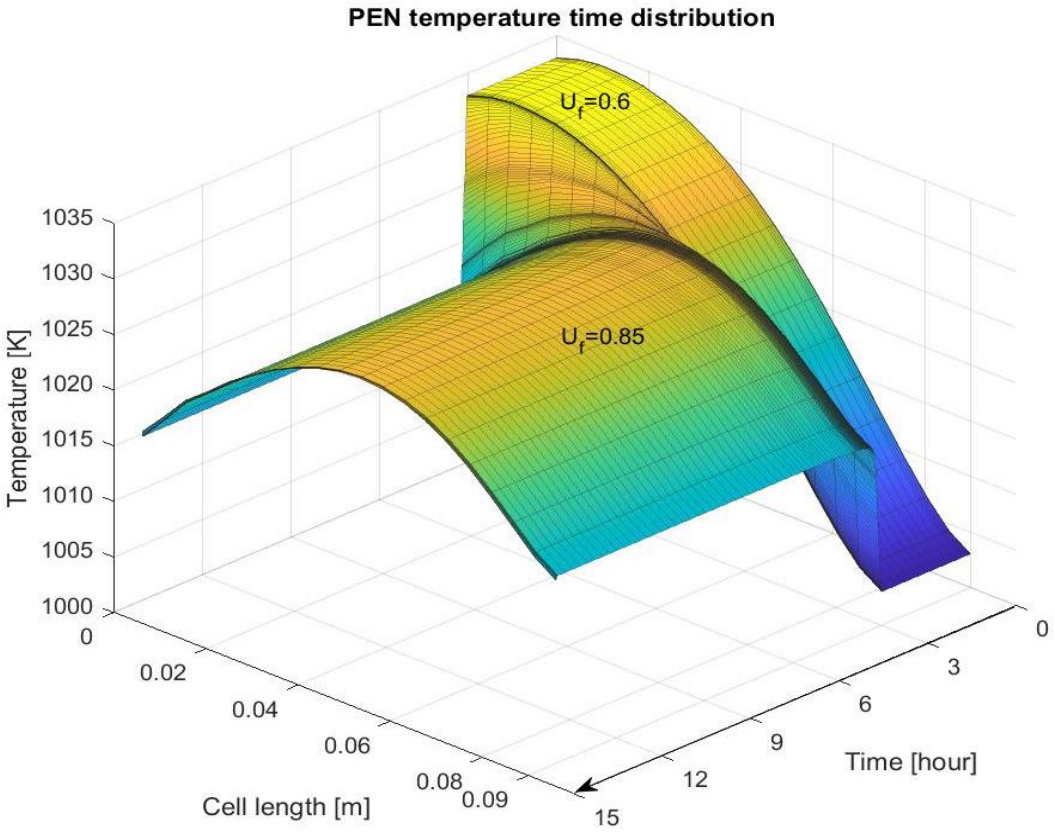


*Figure 31. PEN temperature distribution changes during the transient.*

Therefore, the control of the $\Delta T_{stack}$ with respect to the initial set point can be relaxed, keeping the recommendation previously mentioned. As mentioned in the previous chapters, the thermal stresses in the PEN layer to worry about are not only the longitudinal one (in the direction of the flows into the fuel cell) but also the punctual values in its domain.

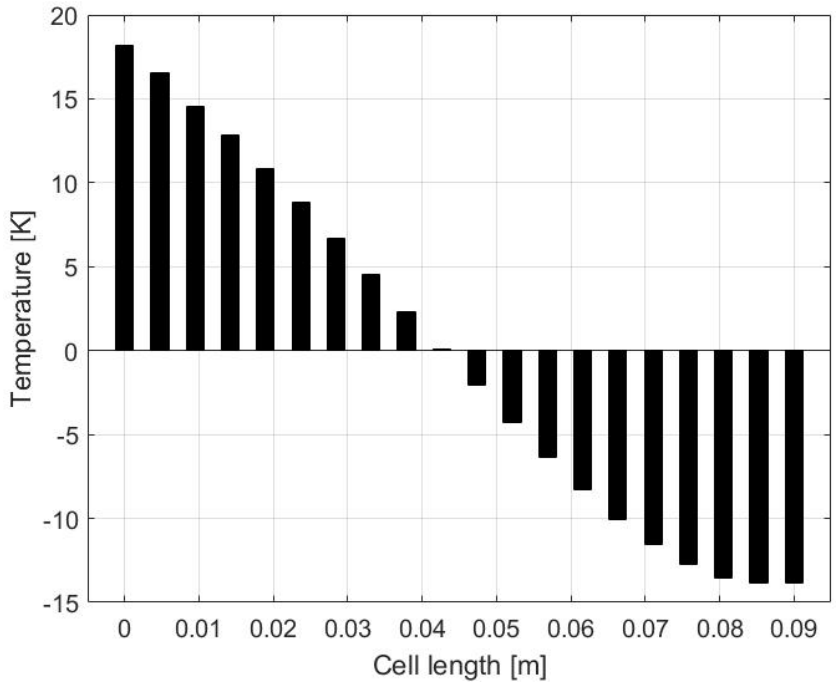


*Figure 32. Local temperature differences inside the fuel cell moving from design condition at Uf=0.6 to the off design at 0.85.*

The values reported in Figure 32 represent the temperature differences in the same point along the 9 cm of the fuel cell, between the initial condition at 0.6 and the new steady state at 0.85. The first half of the fuel cell would be affected by a compression because the temperature decreases while the second part increases. Moreover, this phenomenon regards the PEN layer that is supposed to have a different thermal expansion coefficient with respect to the other layers of the cell [65]. In another study, the FEM results showed that the thermal expansion coefficients mismatch among components affects the thermal stresses distribution more than the temperature gradient alone does [66]. In a continuously dynamic operation between these two configurations, the thermal gradients at the two extremities will affect the mechanical stability of the layer, and it could be one of the limitations of the dynamic $U_f$ operation as confirmed by other works [67] showing the linear dependency of the maximum stress which are expected to be higher at lower utilization factor.

In Figure 33 the temperature of the air showed follows a different trend from the Figure 30 in the HX1 because of the mixing process downstream the heat exchanger. Another strategy for keeping track of the gradient inside the cell is

under evaluation and it would make use of both the cathode temperature difference (that can be controlled by the air flow) and information about the profile expected inside the cell.

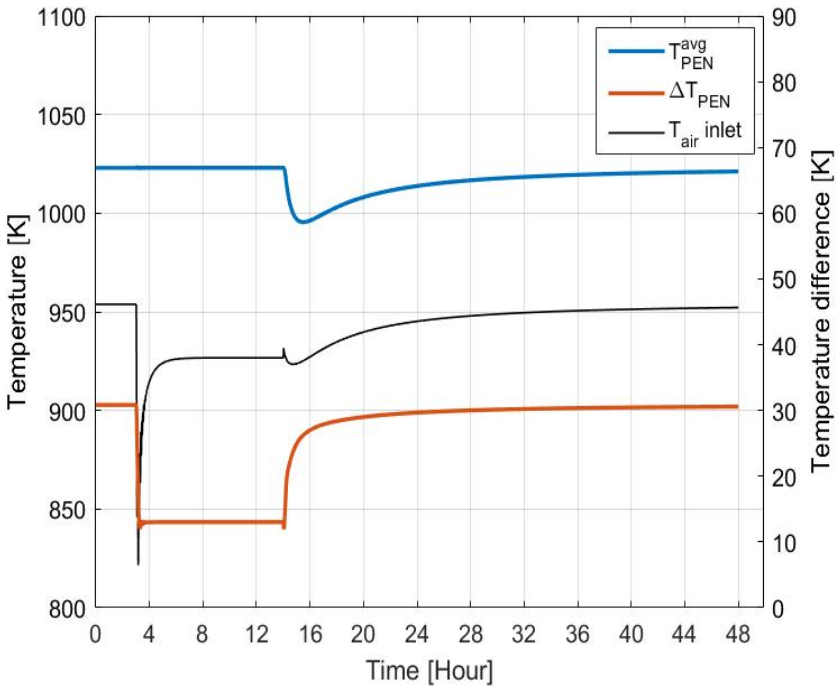


*Figure 33. PEN temperature response (quite constant) and temperature difference controlled across the stack. The black line is the temperature of the air supplied to the SOFC.*

Thus, the hydrogen production can be controlled through the utilization factor, and so processing more or less fuel with respect to the nominal condition. Increasing by 20% the power output of the SOFC, the hydrogen flow at the anode outlet increased more than 20% without substantial change in the anode outlet composition; in the second dynamic, when the $U_f$ increases by 40% with respect the design value, the hydrogen flow reduces more than 70% (!) and the outlet composition is completely different. If the only aspect to be considered was the hydrogen production at the outlet of the SOFC, it is totally clear that the change in fuel utilization is the proper mean and it can be as quick as the fuel processing allows it, even though the performance of the cell might not be completely stable due to the different time constants involved. For this purpose, since the main focus is to stabilize and have a complete control of the hydrogen production that can be seen as "on demand production", the only objective concerning the fuel

cell is to operate in safe conditions avoiding abrupt changes in temperature and limiting the fluctuations in terms of thermal stress.

Once the hydrogen dynamic production has been proved, different logics about its dispatchability can be implemented. The reader should be aware that even though the dynamic production has been demonstrated, the fuel cell that operates in tri-generation mode is not comparable with a simple electrolyzer in terms of productivity and speed in changing the hydrogen production rate, since more variables and phenomena are involved (e.g. SMR, WGS, power as output not input, different current density and temperature profile..).

## 4.3. Co-products controller

An ideal polygeneration plant should be able to regulate each of its products. In this case, power, heat and hydrogen production could be controlled in a different way. Unfortunately, using a SOFC for tri-generation purpose does not allow easily an independent production of power and hydrogen at the same time, because they are related through fuel flow. When the power decreases keeping constant the fuel utilization, the fuel flow needed for the production of that percentage of power is lower than the nominal case, and the amount of hydrogen produced is of course related to the fuel flow processed. One way to do that, is to regulate continuously both power and utilization factor, so that when the power goes down the $U_f$ can go down as well and the fraction of the hydrogen available at the outlet is higher and it compensates the smaller amount of fuel flow. The real actuation of this strategy is very difficult though: first, both the decrease in power and in fuel utilization bring the cell to a lower average temperature so the electrical performance start to get worse; second, the current density distribution inside the fuel cell will be totally unstable, and with that the voltage as well. In the end, the overall thermal and electrochemical features could be very tough to manage even with more variables to be controlled (for example, adding an external heat source that can independently adjust the inlet conditions both on the fuel and air lines).

On the contrary, if the cell works at constant power, the other two regulation have a higher degree of independence. There many ways to design a system that can

control these two co-products, but in this case study the two components assigned to those tasks are the Oxidizer bypass valve and the HSU.

Changing the airflow that bypasses the oxidizer it is possible to change the outlet of the oxidizer in terms of temperature and flow after the combustion (i.e. heat available) as already discussed in the design choice. The hydrogen separation unit choses the amount of hydrogen intended for end use both regulating the operation of the PSA or recirculating part of the incoming anode exhaust. A graphical representation is provided in the Figure 34, where the three products of the plant constitute the three axes of the plot and the design condition (i.e. at 0.6 utilization) is depicted as a sphere that could be moved in the 3D space. Again, keep in mind that the regulation of the power axis does not allow an independent regulation on the other two. Therefore, even in a 3D space, there is a sort of domain in which the plant can operate.

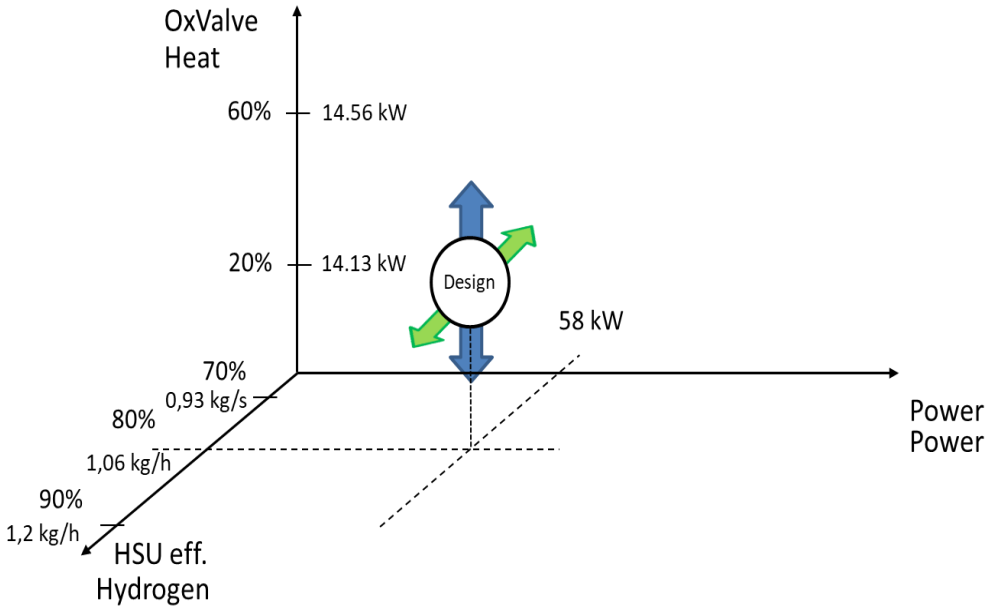


*Figure 34. 3D domain of the co-products control. The power is not an independent regulation as the other two variables.*

## 4.4. Performance indexes

In the polygeneration analysis, the definition of the system efficiency calculation matters because it shows the advantage of producing more than one product from the same plant and energy input. One of the best methodologies to analyze

polygeneration plants is through a techno-economic assessment using exergo-economic method ([26], [68], [69]). The outcomes of this analysis are usually expressed in terms of unit cost of production for each product of the polygeneration plant, giving some clues on its feasibility and convenience. In this study, the economic analysis has not been considered, therefore the system efficiency and the Primary Energy Savings (PES) are the only parameters able to express a performance index of the plant.

The work of Brouwer et al. [45] provides a methodology called Supplemental Inputs Method able to allocate a share of the total input energy flow to the production of each co-products. The idea of this method is to divide the total energy input into different contributions to generate on purpose each product of the polygeneration plant, supposing that each output can be directly evaluated. The advantage of the method lies in the generalization procedure useful for comparative analysis among different technologies if the same outputs should be evaluated. The common variables with which the efficiencies can be compared are listed in Table 14 and refers to the state-of-the-art technologies used to produce those co-products.

| Comparable $\eta$ considered | Value | Comments |
|---|---|---|
| Power Plant efficiency $\eta_{PP}$ | 0.47 | Distributed electricity generation using a stand-alone HTFC without poly-generation or co-generation |
| | 0.60 | Typical modern natural gas combined cycle plant |
| Boiler efficiency $\eta_{boiler}$ | 0.60 | Fueled boiler at less than full load |
| | 0.85 | Natural gas boiler at full load |
| Chemical plant efficiencies $\eta_{cp}$ | 0.79 | Centralized steam methane reformation (SMR) to produce pure hydrogen from natural gas |
| | 0.65 | Centralized methanol production from natural gas |
| | 0.65 | Distributed SMR to produce pure hydrogen |

*Table 14. Conventional state-of-the-art efficiencies from* [45]

In this work, the polygeneration plant consists of three products, so the definitions of electrical, thermal and chemical efficiencies are presented in the following equations:

$$\eta_{el} = \frac{P_{net}}{E_{e^-}} = \frac{P_{net}}{E_{tot} - \frac{Q_{e^-}}{\eta_{boiler}} - \left( \left( U_f - U_{f,H_2} \right) \cdot E_{tot} + \frac{P_{PSA}}{\eta_{CC}} \right)} \tag{47}$$

$$\eta_{th} = \frac{Q_{net}}{E_Q} = \frac{Q_{e^-} + E_{burner} \cdot \eta_{burner}}{\frac{Q_{e^-}}{\eta_{Q_{e^-}}} + E_{burner}} = \eta_{Q_{e^-}} \tag{48}$$

$$\eta_{ch} = \frac{H}{E_c} = \frac{H}{\left( U_f - U_{f,H_2} \right) \cdot E_{tot} + \frac{P_{PSA}}{\eta_{CC}}} \tag{49}$$

Concerning the Eq. (47), the electrical efficiency is defined as the ratio of the net electrical power over the net energy input used for electricity purpose: so, in the denominator the quantity related to the heat and hydrogen production has been subtracted. The $P_{net}$ is the output of the fuel cell minus the consumption of the blower and PSA. The same logic applies to the other two efficiencies, but there are at least two important comments. First, the $\eta_{th}$ results to be equal to $\eta_{Q_{e^-}}$ because this layout has been designed to work without other external heat sources (indeed there is a net cogeneration), so the supplemental heat supplied, $E_{burner}$, is zero. The $\eta_{Q_{e^-}}$ corresponds to the thermal efficiency associated with the electricity production, as defined by the authors. This quantity cannot be directly measured or estimated because it comes out as output of the fuel cell thermodynamics and electrochemistry, and the authors suggested to assume that value equal to $\eta_{boiler}$. Actually, it can be assumed equal to 1, since the energy input related to the heat generation only is equal to zero, because is the same input used for electricity production, but the system is designed in order to be able to use that available heat downstream. The second comment regards the Eq. (49), because the energy input in this case is represented by two terms: the first one is the difference between the utilization factor used without aiming to produce hydrogen (i.e. standard cogeneration concept, assumed to be equal to 0.85) and the utilization factor employed for tri-generation purpose (i.e. hydrogen

production) which is the one of the design case (0.6). This difference is then multiplied by the total energy input $E_{tot}$, defined as:

$$E_{tot} = \dot{m}_{fuel,in} \cdot LHV_{fuel} = 124.6\ kW \tag{50}$$

The second term is an "electrical energy" contribution represented by the consumption of the PSA. Since the PSA consumption would not have been present if the hydrogen was not produced, it means that is an energy input related to the hydrogen production. In this case the reference efficiency for the power absorbed by the PSA is the efficiency of a combined cycle power plant in Table 14. The chemical output $H$ is instead the mass flow of hydrogen produced multiplied by its LHV, and it is equal to 35.4 kW.

In future works, is strongly recommended to include a dynamic HSU model (PSA included) in order to simulate the overall plant dynamically. For the efficiency calculation purpose, two reasonable values of PSA consumption have been considered: 17% of the nominal SOFC power (58 kW) [70] in similarity with the consumption emerged from OCSD case, and a value of 15% that comes from the curve fit in Eq. (51) used in previous work [71] considering the hydrogen concentration at the inlet of the HSU and multiplied by the hydrogen production of 2.95e-04 kg/s per module:

$$E_{H_2,HSU} = 11.613 \cdot \chi_{H_2}^{-1.123} \qquad \left[\frac{MJ}{kg_{H_2}}\right] \tag{51}$$

Using the first reference, the $P_{net}$ is equal to 46.3 kW, therefore the electrical and chemical efficiencies are listed below:

| $P_{PSA,17\%}$ | $P_{PSA,15\%}$ |
|---|---|
| $\eta_{el} = 76.7\ \%$ | $\eta_{el} = 76.1\ \%$ |
| $\eta_{ch} = 74.5\ \%$ | $\eta_{ch} = 77.6\ \%$ |
| $\eta_{mix} = 76.9\ \%$ | $\eta_{mix} = 77.9\ \%$ |

*Table 15. Efficiencies of the system with Supplemental Input Method in design condition (tri-generation).*

The last row, called total mixed efficiency, represent the overall efficiency of the plant just summing up the three co-products (i.e. $P_{net}$, $Q_{net}$, $H$) and dividing them

by the total energy input $E_{tot}$. Even though the difference between the two references in the PSA consumption is only of 2 %, the efficiencies of the system change: the convenience of this powerful method shows that if the consumption of the PSA decreases, the efficiency related to the electricity production increases less than the increase verified in the hydrogen production. The explanation lies on the definition of SIM itself, because since the PSA consumption is attributed to the hydrogen production, the chemical efficiency is sensible to its variation. The other consideration is that the hydrogen fraction in the mixture going to the HSU is very important to lower the consumption of the PSA. The total mixed efficiency of this study is totally comparable with the mentioned work [71] considering the tri-generation operation with HTFC.

Another important performance index related to the efficiency just presented, is the Primary Energy Savings defined by the Direttiva 2004/8/CE as the primary energy that could be saved if the same outputs were produced by state-of-the-art technologies, which are the natural gas combined cycle plant, distributed SMR hydrogen production and natural gas fed boiler (the value in the brackets refers to the second reference for PSA consumption of 15%).

$$PES = \frac{\frac{P_{net}}{\eta_{CC}} + \frac{H}{\eta_{SMR}} + \frac{Q_{net}}{\eta_{boiler}} - E_{tot}}{\frac{P_{net}}{\eta_{CC}} + \frac{H}{\eta_{SMR}} + \frac{Q_{net}}{\eta_{boiler}}} = 16\ \% \qquad (17.1\%) \qquad (52)$$

This index gives a quick shot about the convenience of this tri-generation plant for dynamic hydrogen production with SOFC. Although this index has been initially established for co-generation system only (power and heat) by the cited directive, it gives a precise evaluation about how much primary energy can be saved concentrating multiple products in the same plant, starting from the same input.

# 5. Considerations about reference studies

In the following two paragraphs, there are few considerations *a posteriori* about the two motivations on which this study has been thought.

## 5.1. MCFC case in OCSD

The world's first tri-generation plant has been installed in the Orange County Sanitation District's wastewater treatment plant in Fountain Valley, California [72]. The fuel cell used at that time was a molten carbonate fuel cell, that usually operates at lower temperature with respect to the solid oxide fuel cell, and its electrical performance are worse than SOFCs. The concept of the plant was almost the same adopted in the current study, even though the layout and the installed capacity (i.e. 300 kW) were different.

*Figure 35. First tri-generation plant in the world using a MCFC in a WWTP.*

In this paragraph the emphasis is on the specific hydrogen production of the plant, highlighting the different performance that a tri-generation plant based upon SOFC would have. It is right to specify that the two fuel cells are completely different and their working conditions as well, so a quantitative direct comparison is meaningless. According to Kast's records of the plant [70], the hydrogen production on 7/28/2011 was 4.85 kg/h with a fuel utilization of 0.62 and at current density equal to 0.12 A/cm$^2$. The yield of hydrogen production with respect to the installed capacity for the MCFC is defined as:

$$Yield_{MCFC} = \frac{H_{2,day}}{Power} = 0.38 \left. \frac{kg_{H_2}}{day} \right/ kW \quad (53)$$

In the current study, the SOFC model in design condition at $U_f$ equal to 0.6 and 0.25 A/cm$^2$ would have a different yield:

$$Yield_{SOFC} = \frac{H_{2,day}}{Power} = 0.44 \left. \frac{kg_{H_2}}{day} \right/ kW \quad (54)$$

This difference cannot be explained just by the comparison of the two different type of fuel cells, because the operating conditions are different and the system layout as well. However, if the SOFC and the MCFC had the same fuel inlet, the same utilization factor and current density in design condition, the solid oxide fuel cells would have a better ratio hydrogen production/fuel input simply because the higher temperature fosters the SMR reaction and the hydrogen concentration at the exit will be higher. In any case, the adoption of a molten carbonate cell has other benefits such as the possibility to recover the $CO_2$ even though the electrical efficiency is lower [44].

## 5.2. DEMOSOFC further development: from co-generation to tri-generation plant

The potential of the tri-generation concept applied to the outstanding results of the DEMOSOFC project, the first example in Europe of high efficiency cogeneration plant with a medium size fuel cell fed by biogas, it could represent a further development of fuel cells installations in WWTPs. The Collegno facility has a maximum capacity of 270,00 P.E (equivalent inhabitants – *persone equivalenti in italian*) able to collect 59,000 m$^3$ of wastewater, although it is now on service of smaller amount of P.E. [62].


*Figure 36. DEMOSOFC plant located in Collegno in SMAT wastewater treatment plant* [73]*. Two of the three Convion® modules are depicted on the right.*

The SOFC modelled in the current work is different from the Convion® cells installed in Collegno, so the values obtained from the simulations cannot be directly compared with data measured on the plant: although this is a weak point of the study because the SOFC technical specifications are not public, it is reasonable to think about installations of the commercial fuel cell modelled. In that case, the amount of biogas required by the three modules of 58 kW each for tri-generation would be about +23% because the utilization factor is lower than the one used in DEMOSOFC. Thus, considering the average biogas flow rate produced by the facility in 2015 that is 71.58 $Nm^3/h$, it is still possible to install three modules which operate in tri-generation mode. However, one way to optimize the number of modules that can be installed might be discretizing the biogas production profile, as shown in Figure 37, and identifying several steady states (red discretization) or a very slow dynamic profile (yellow discretization) in which a combination of a certain number of modules (at different loads) need to operate.

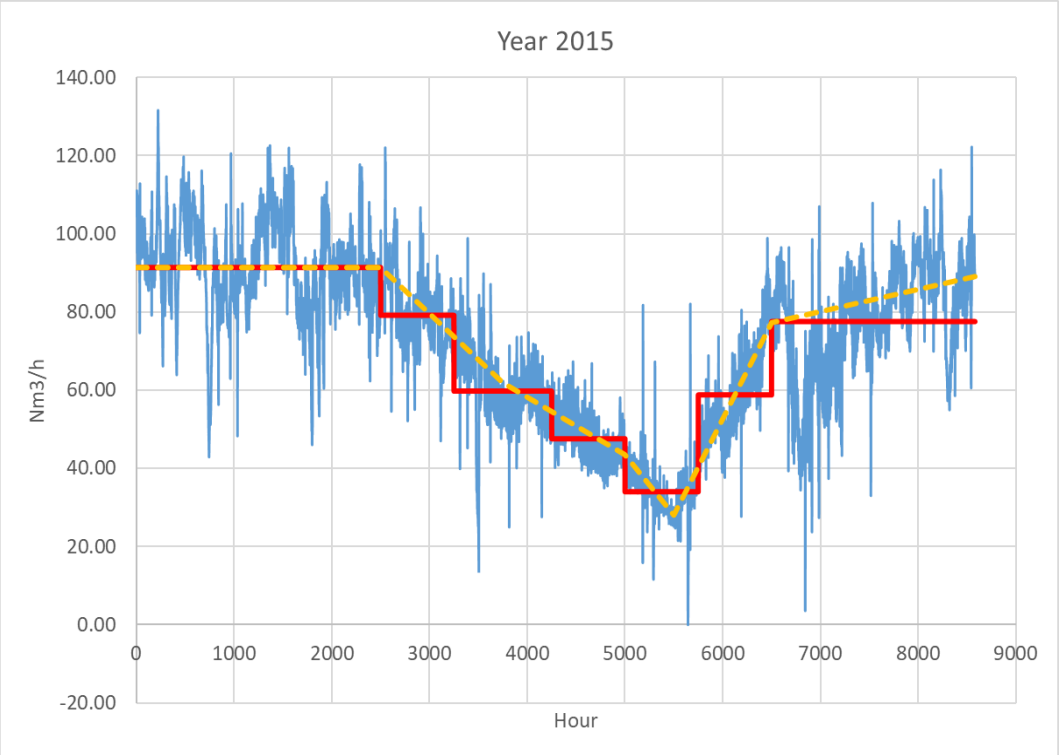


*Figure 37. Biogas hourly production in 2015* [36] *discretized by the author.*

For example, considering the red discretization, in summertime the biogas production reaches its minimum mainly because lower incoming wastewater. In that period, the biogas production can be averaged on a month from mid of July to mid of August around a rate of 34 $Nm^3/h$ whereas a single module from the current study should require 20.8 $Nm^3/h$ of biogas at full load in tri-generation mode and may be combined with another module at 61% power load that consumes only 12.6 $Nm^3/h$, without shifting the mode to cogeneration at $U_f$ equal to 0.85 (as described during the dynamic results presentation). From the conclusions about the dynamic of the utilization factor, that it should be quite slow to avoid fast change in the temperature profile of the cell and limiting stresses inside the layer, the yellow discretization (i.e. linear discretization) can also be followed. An algorithm to optimize the operation of the three modules together during the whole year, having every time the best combination of the three modules could be an interesting method to implement.

The layout design has been justified along the chapters, but this choice should not be seen as a limitation. Carrying out an economic analysis on the cost of production of the hydrogen (and its final price considering its end-use) and on the

savings in terms of electricity production from the SOFC intended for internal use of the WWTP, it may turn out to be better producing more hydrogen at the expense of the other two products. Therefore, other layouts for utilization factors lower than 0.6 should be considered (i.e. going down in the endothermic condition of the fuel cell, where the inlet temperature of the streams has to be higher than the average of the fuel cell because the SOFC requires heating and not cooling!) developing the plant in a tri-generation system without a net cogeneration (it means that the heat available would be used only to partially warm up the incoming streams and not for the sludge line heating). The best choice would be rethinking about the HXs coupling, but the easiest choice consists in adding two external heat sources on the fuel and air lines before the SOFC, as shown in Figure 38, to manage the increase in temperature if the fuel cell works with $U_f < 0.6$. For example, from the sensitivity analysis explored in the first part of the work, the change in hydrogen production was more than doubled when the fuel utilization went down to 0.4.

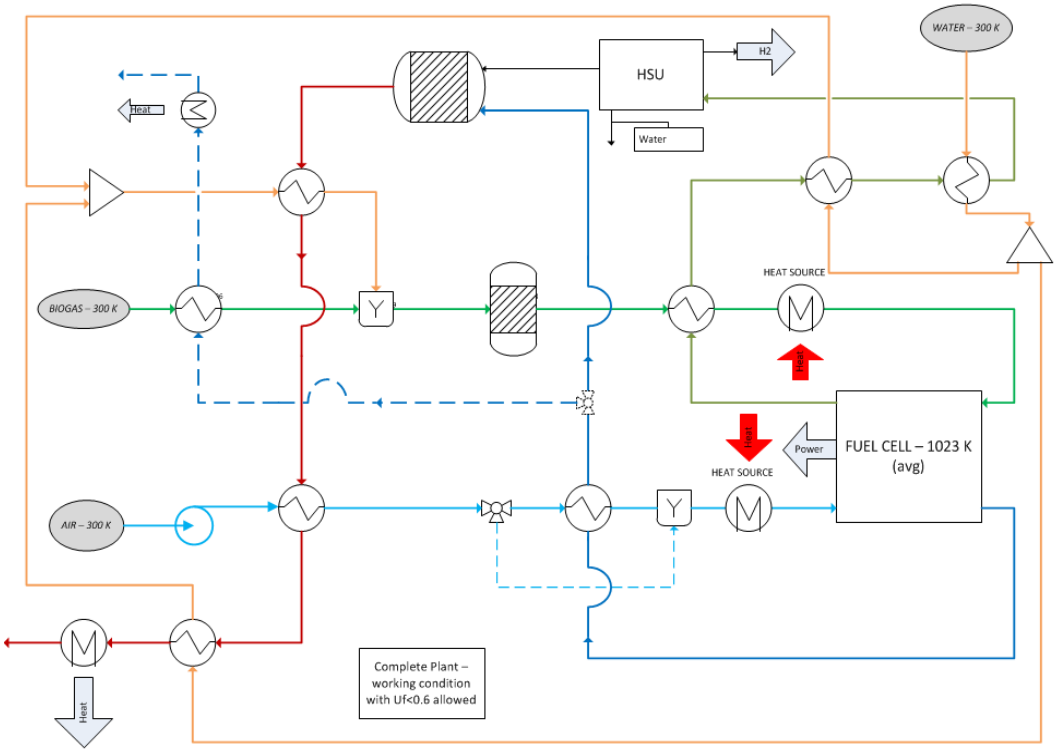


*Figure 38. Tri-generation plant with external heat sources to operate the SOFC below the thermoneutral condition.*

# 6. WWTPs as distributed infrastructure

The importance of the hydrogen towards a society no longer based on fossil fuels consumption, aiming to reduce GHG and criteria pollutant emissions, is crucial as described in the introduction. Its flexibility is one of the main advantages because it can be used in different sector and with different technologies, with the fuel cells that will have certainly a primary role.

California is one of the leading states in US and in the world in terms of clean energy conversion and hydrogen uses (few examples provided in Chapter 1). The P2G concept is one of the most pursued topics from researchers and companies because it has already been proved to be the most cost-effective solution for long-term energy storage. Furthermore, the conversion of some technologies (from domestic cooking burners to gas turbine power stations) has been studied to be compatible if a certain percentage of hydrogen is included in the supply, once its injection into the pipeline becomes effective on a regional or national scale, allowing direct use other than the purpose of seasonal conservation. Moreover, California has also the most developed market in terms of FCVs travelling on the roads thanks to the quite high number of hydrogen fueling stations available, as shown in Figure 39 and Figure 40 [8].

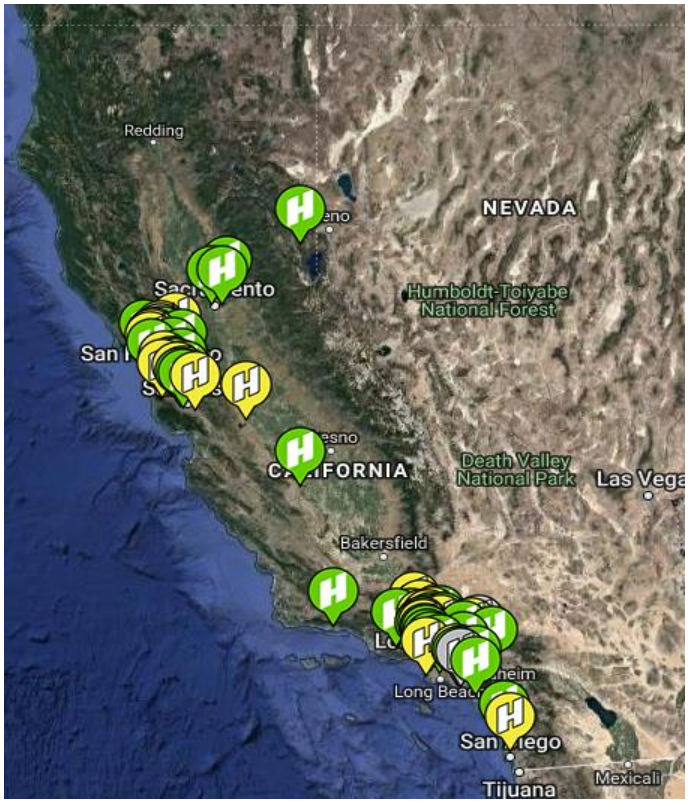


*Figure 39. California Hydrogen fueling stations. Largely spread in the San Francisco bay and Los Angeles area. Green icons represent the ones in operation, whereas yellow and grey in commissioning or temporary closed.*

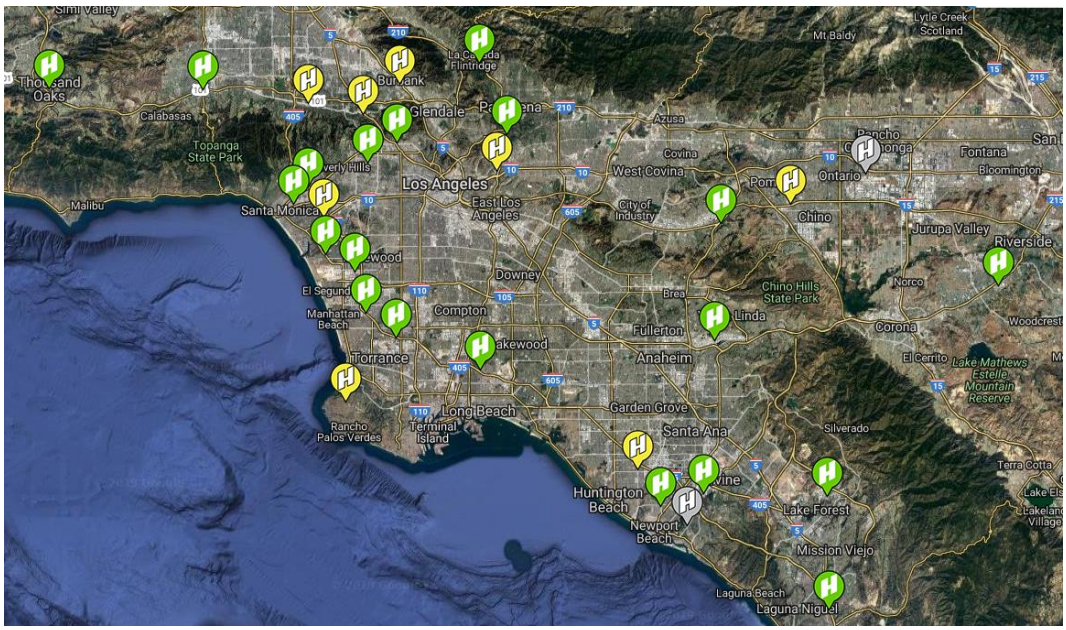


*Figure 40. Zoom on Los Angeles area. The Orange County is a fertile land to continue the expansion of hydrogen infrastructure.*

At the end of September 2019, there are 41 stations opened to the public and more the 20 planned or under construction. At the end of the 2020, 64 hydrogen

stations are expected to be opened to the public according to the California government.

The potential tri-generation installations in WWTPs could be a very important addition to the ones already mentioned, considering all the benefits that their installations have also for the plants themselves. In Figure 41, the biggest WWTPs along the Californian coast are depicted and some of them could be integrated as part of the hydrogen fueling stations infrastructure [74].

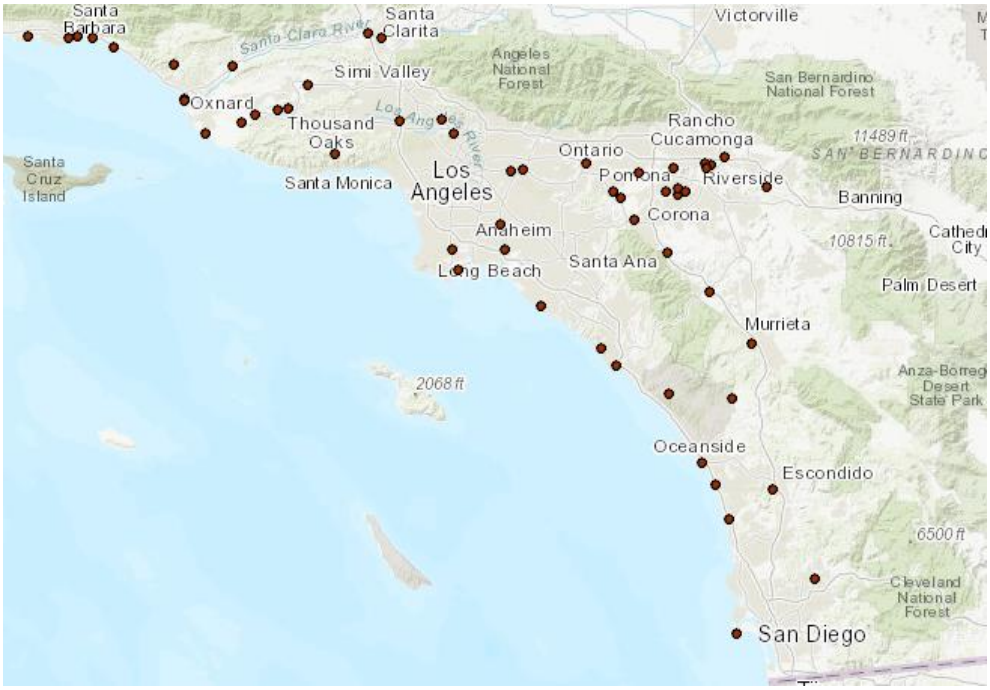


*Figure 41. Southern California main WWTPs on the coast. Image from databasin.org based on Pacific Institute study upon risk of flooding due to sea level rise.*

Unfortunately, there is not a Californian database about wastewater treatment plants as for Europe (eea.europa.eu – UWWTD database), and the estimation of the potentiality should be studied separately, collecting data from each plant and to evaluate the possible installation of third treatment with AD where is not done. However, the same yield of biogas production of an Italian WWTP (e.g. Collegno) according to the size of the plant (in Europe expressed by P.E.) cannot be applied to the California case because the management of the wastewater is done in a different way with respect to the standard Italian methods. The main difference regards different treatment to which the "white" water and "black" water are subjected: the first one, are mainly made by water coming from natural

phenomena instead the second one, with a very high COD, coming from waste water of human activity strongly influenced by the use of the garbage disposal. Although this could be an advantage on the biogas production through AD because of higher yield with respect to the incoming amount of water that needs to be treated, a separated investigation is necessary.

The Italian situation is quite different because the only public hydrogen fueling station opened to the public is in Bolzano. The lack of hydrogen infrastructure could be interpreted as a motivation to start spreading FCVs use relying on installations in WWTPs across the country. The preliminary case study presented herein assumes that the yield of biogas production with respect to the size of the plant is constant, and equal to the yield of the WWTP located in Collegno where DEMOSOFC modules are installed. Although this is a limiting assumption because the biogas production rate is strongly influenced by the boundary conditions of the plant (such as location, weather, anthropogenic activity) which influence the composition of the wastewater and consequently the yield of the biogas production with respect to the size (i.e. P.E.), the actual value of the Collegno plant is below the Italian average. Therefore, the estimation provided at the end of this chapter is conservative enough to understand the importance of having tri-generation plants dislocated all over the country.

From the biogas production data of two years (2015,2016) the average biogas production over the whole year produces 608,294 $Nm^3$ per year [33]. Right now, the plant is serving 180,000 P.E. and its biogas yield with respect to the size of the plant is 3.38 $Nm^3$/year/PE. This value allows the installation of three tri-generation modules, even though no optimization logic has been applied as in the design of DEMOSOFC project, and with this methodology it has been possible to identify the minimum size of the WWTP that permits the installation of at least one tr-generation module of 58 k, according to the simulations result. The minim number that came out is 60,000 P.E. (reasonably expected since base on DEMOSOFC design condition) for a total 226 plants eligible in the entire country. Thanks to the database mentioned earlier, in Italy the location of the WWTPs is easier than California , and they come together with information about their size in terms of P.E (Figure 42).


*Figure 42. Italian WWTPs location above 60,000 P.E.*

Another constraint consists in the use of 58 kW as a minimum size of the module: although is reasonable that for very small plants could be economically difficult to install a biogas production system, this should not be taken as conclusion a priori without performing and economic study on that (suggested for future works). Once clarified the assumptions (and limits) of this evaluation, in the following table the total amount of power installable and hydrogen possible production are listed.

| | |
|---|---|
| Total power installation in WWTPs | 32.07 MW |
| Total tons of $H_2$ production in one year | 4365 $ton_{H_2}$[1] |
| Total SOFC modules | 553 |

*Table 16. Results for the case study based on Collegno yield and current work simulations.*

[1] A capacity factor of 85% has been assumed for those plants.

Obviously, because of the lower bound regarding the size of the plants, the highest concentration of the red dots representing the WWTPs is around the biggest cities which means higher population and anthropogenic activities. For this reason and for the lack of a developed infrastructure, one of the best intended use is for car sharing mobility with FCVs because the travelled distance is limited, the car sharing use is mostly concentrated in big cities and the intermittency of the use allows the refueling in the hydrogen stations close to the WWTPs [75]. For example, from the map the areas most suitable for this application are Torino and Milano. According to [76], in 2016 the average distance travelled for each rental in Torino was 5.3 km and in Milano 7.2 km. Considering the two most used cars in California, Toyota Mirai and Honda Clarity, they both have a consumption of 66 miles (106 km) per kg of hydrogen, considering a mix track of highway and city roads [10]. It means that in Torino for each kg of hydrogen produced, it is possible to feed 20 rentals with FCVs or almost 15 in Milano where each car has an average of 5.1 rentals per day (considering a fleet of about 3000 cars), therefore each kg of hydrogen is able to fill 3 cars per day with the car sharing use described.

*Table 17. Hydrogen fueling station representation from Toyota's website.*

Another point of view could be the calculation of the total number of full refueling for each car, for a given tri-generation plant: Toyota Mirai has a capacity tank of 4.7 kg, that according to EPA the full refill would cost less than 26 $ (around 5.5 $/kg [10]). Since the current study simulations for a Collegno size plant showed a production of 76.3 kg/day for three modules, the tri-gen installation described

could feed up to 16 Mirais per day, which is a very impressive number for car sharing purpose. In Torino, 16 Mirais are enough to guarantee more than 1,500 rentals per day!

The prospective just provided should not be considered as a methodic study upon the potential that a distributed infrastructure has, based on hydrogen production tri generating SOFC fed by biogas, but it certainly provides a rough estimation about what Italy might offer in a hydrogen-based society for the next decades.

# 7. Conclusions

The description of a dynamic model of a high temperature fuel cell has been largely described in the current work, highlighting how the performance of the SOFC are extremely advantageous as energy conversion device. Moreover, the synergistic effect of the tri-generation concept for a HTFC fed by biogas coming from waste products enhances the motivations for installing SOFC modules able to produce electricity, heat at high temperature, and hydrogen. The necessity of a spatially resolved model has been justified in order to understand the main problem that occurs in the fuel cell regarding the temperature drop at the very beginning of the anode channel, due to the SMR endothermic reaction, and a control strategy has been adopted to operate the fuel cell dynamically in safe conditions. The PI controller reacted well in controlling the two variables (air flow, air inlet temperature) in order to maintain the set points of the cell. After a sensitivity analysis on the $U_f$, the benefits of the thermoneutral voltage as operating condition for the fuel cell have been presented and consequently the choice of fuel utilization factor equal to 60% was used for the design condition. In the design condition the hydrogen concentration at the anode outlet is 21.8% accounting for a 1.32 kg/h hydrogen mass flow, and consequently separated by the HSU with assumed efficiency of 80%. During the steady states studies, the main efforts in the design were to reduce consumption of blower (thanks to the minimum air flow provided), improving the hydrogen production, and exploit the heat recovery from the system. Two dynamics have been explored: changing the power output of the fuel cell and its fuel utilization factor. In both cases the SOFC controller was able to prevent risky thermal gradient of the cell and stabilizing the cell in a new steady state condition. Running the dynamic simulations, the importance of certain elements like the interconnector came out: its thickness is a very important parameter in dynamic simulations, because it changes a lot the thermal capacity of the whole cell and its behavior during transient, and it should be taken into account in the design of fuel cell according to the operation conditions that the SOFC will face. With the layout presented, the regulation of each of the three products was possible, even though a change in the electricity production will affect the other two co-products. Using the SIM, the electrical and

chemical efficiencies of the tri-generation plant have been calculated and compared with the state-of-the-art technologies showing a PES of 16%. With the hydrogen production from tri-generation plant installed in WWTPs, using renewable biogas, different final uses were described. Some of them in some countries are still not mature to justify investments on that way, but the use in the FCVs for mobility purpose has been identified as the most viable solution. For the Italian case study, the total amount of hydrogen produced over a year with 553 modules as the one simulated in the work is around 4365 tons, accounting for 523 TJ of clean energy that can be used in several ways. The car-sharing option, because of the WTTPs location near the big cities and the hydrogen production per hours, has an incredible potential to start developing a hydrogen infrastructure and use.

As final conclusion of the work, there are some suggestions for future works and few aspects that needs to be evaluated in more detailed separate studies: a validation with Convion® fuel cell data is strongly suggested if a solid link from DEMOSOFC project and tri-generation plant in WTTP wanted to be created; a complete dynamic model, which includes PSA, pre-HXs, pre-reformer models will provide a better comprehension of the overall dynamic especially regarding the possibility of controlling each of the product; first, an economic analysis of the tri-generation plant to prove its feasibility, and then elaborating an economic dynamic model in order to catch at each time which is the main product (out of three) that needs to be regulated in order to increase its production. For this last purpose, other layouts could be more interesting to enlarge the window of fuel utilization factor also below 0.6.

# References


[1] M. V. S. Ranganadham, "Energy Statistics," p. 101, 2018.

[2] "Global Energy & CO2 Status Report." [Online]. Available: https://www.iea.org/geco/emissions/.

[3] "Kyoto Protocol - Targets for the first commitment period." [Online]. Available: https://unfccc.int/process-and-meetings/the-kyoto-protocol/what-is-the-kyoto-protocol/kyoto-protocol-targets-for-the-first-commitment-period.

[4] "Paris Agreement, COP21." [Online]. Available: https://ec.europa.eu/clima/policies/international/negotiations/paris_it.

[5] "Tokyo Aims to Realize 'Hydrogen Society'by 2020," 2016. [Online]. Available: https://www.japan.go.jp/tomodachi/2016/spring2016/tokyo_realize_hydrogen_by_2020.html.

[6] "Tokyo 2020 Olympic Games to use hydrogen fuel," 2019. [Online]. Available: https://www.gasworld.com/tokyo-2020-olympic-games-to-use-hydrogen-fuel-/2016200.article.

[7] "Alstom presents hydrogen train in six federal states in Germany." [Online]. Available: https://www.alstom.com/press-releases-news/2019/1/alstom-presents-hydrogen-train-six-federal-states-germany.

[8] "California hydrogen stations." [Online]. Available: https://cafcp.org/stationmap.

[9] Hernandez, Aguiar-Curry, and Wood, "Senate Bill No. 1023," *Calif. Legis. Inf.*, no. 100, 2018.

[10] "EPA." [Online]. Available: https://www.fueleconomy.gov/.

[11] "BP Statistical Review of World Energy Statistical Review of World," 2019.

[12] A. Saeedmanesh, M. A. Mac Kinnon, and J. Brouwer, "Hydrogen is essential for sustainability," *Curr. Opin. Electrochem.*, vol. 12, pp. 166–181, 2018.

[13] N. L. Garland, D. C. Papageorgopoulos, and J. M. Stanford, "Hydrogen and fuel cell technology: Progress, challenges, and future directions," *Energy Procedia*, vol. 28, pp. 2–11, 2012.

[14] J. D. Holladay, J. Hu, D. L. King, and Y. Wang, "An overview of hydrogen production technologies," *Catal. Today*, vol. 139, no. 4, pp.

244–260, 2009.

[15] T. Sinigaglia, F. Lewiski, M. E. Santos Martins, and J. C. Mairesse Siluk, "Production, storage, fuel stations of hydrogen and its utilization in automotive applications-a review," *Int. J. Hydrogen Energy*, vol. 42, no. 39, pp. 24597–24611, 2017.

[16] I. K. Muritala, D. Guban, M. Roeb, and C. Sattler, "High temperature production of hydrogen: Assessment of non-renewable resources technologies and emerging trends," *Int. J. Hydrogen Energy*, no. xxxx, Sep. 2019.

[17] O. V. Marchenko and S. V. Solomin, "Modeling of hydrogen and electrical energy storages in wind/PV energy system on the Lake Baikal coast," *Int. J. Hydrogen Energy*, vol. 42, no. 15, pp. 9361–9370, 2017.

[18] "Greening the grid." [Online]. Available: https://news.uci.edu/2017/01/03/greening-the-grid/.

[19] "UC Irvine injects P2G green hydrogen into campus power supply," *Fuel Cells Bull.*, vol. 2017, no. 1, p. 10, 2017.

[20] A. Cioffi and J. Chatzimarkakis, "Snam : Europe ' s first supply of hydrogen and natural gas blend into transmission network to industrial users," no. April, pp. 1–2, 2019.

[21] P. Margalef, T. M. Brown, J. Brouwer, and S. Samuelsen, "Efficiency comparison of tri-generating HTFC to conventional hydrogen production technologies," *Int. J. Hydrogen Energy*, vol. 37, no. 12, pp. 9853–9862, 2012.

[22] Y. Shiratori, T. Ijichi, T. Oshima, and K. Sasaki, "Internal reforming SOFC running on biogas," *Int. J. Hydrogen Energy*, vol. 35, no. 15, pp. 7905–7912, Aug. 2010.

[23] J. Van Herle, Y. Membrez, and O. Bucheli, "Biogas as a fuel source for SOFC co-generators," *J. Power Sources*, vol. 127, no. 1–2, pp. 300–312, Mar. 2004.

[24] B. Shaffer and J. Brouwer, "Feasibility of solid oxide fuel cell dynamic hydrogen coproduction to meet building demand," *J. Power Sources*, vol. 248, no. 2014, pp. 58–69, 2014.

[25] D. Mogensen, J. D. Grunwaldt, P. V. Hendriksen, K. Dam-Johansen, and J. U. Nielsen, "Internal steam reforming in solid oxide fuel cells: Status and opportunities of kinetic studies and their impact on modelling," *J. Power Sources*, vol. 196, no. 1, pp. 25–38, 2011.

[26] M. Yari, A. S. Mehr, S. M. S. Mahmoudi, and M. Santarelli, "A comparative study of two SOFC based cogeneration systems fed by municipal solid waste by means of either the gasifier or digester," *Energy*, vol. 114, pp. 586–602, Nov. 2016.

[27] A. Hagen, H. Langnickel, and X. Sun, "Operation of solid oxide fuel cells with alternative hydrogen carriers," *Int. J. Hydrogen Energy*, vol. 44, no. 33, pp. 18382–18392, Jun. 2019.

[28] T. P. Holme, R. O'Hayre, S. W. Cha, W. Colella, and F. B. Prinz, *Fuel cell fundamentals, Solutions*. 2006.

[29] L. Mastropasqua, A. Donazzi, and S. Campanari, "Development of a Multiscale SOFC Model and Application to Axially-Graded Electrode Design," *Fuel Cells*, vol. 19, no. 2, pp. 125–140, 2019.

[30] H. Madi *et al.*, "Solid oxide fuel cell anode degradation by the effect of siloxanes," *J. Power Sources*, vol. 279, pp. 460–471, Apr. 2015.

[31] V. Chiodo *et al.*, "Biogas reforming process investigation for SOFC application," *Energy Convers. Manag.*, vol. 98, pp. 252–258, Jul. 2015.

[32] A. H. A. Lanzini, M. Gandiglio, A. Le Pera, M. Santarelli, E. Lorenzi, T. Hakala, "DEMOnstration of large SOFC system fed with biogas from WWTP, Energy planning of the DEMO," vol. Deliverabl, no. 2, pp. 1–27, 2016.

[33] M. S. Polito and U. Fausone, "Project n° 671470. ' DEMOnstration of large SOFC system fed with biogas from WWTP ,'" no. 3, 2017.

[34] "Fuel cells and hydrogen Joint Undertaking." [Online]. Available: https://www.fch.europa.eu/page/who-we-are.

[35] S. A. Saadabadi, A. Thallam Thattai, L. Fan, R. E. F. Lindeboom, H. Spanjers, and P. V. Aravind, "Solid Oxide Fuel Cells fuelled with biogas: Potential and constraints," *Renew. Energy*, vol. 134, pp. 194–214, 2019.

[36] M. Gandiglio, P. Torino, A. Lanzini, P. Torino, and P. Torino, "Industrial Size Biogas Sofc System in a Wastewater Treatment," 2018.

[37] A. S. Mehr *et al.*, "Solar-assisted integrated biogas solid oxide fuel cell (SOFC) installation in wastewater treatment plant: Energy and economic analysis," *Appl. Energy*, vol. 191, pp. 620–638, 2017.

[38] A. A. Trendewicz and R. J. Braun, "Techno-economic analysis of solid oxide fuel cell-based combined heat and power systems for biogas utilization at wastewater treatment facilities," *J. Power Sources*, vol. 233, pp. 380–393, 2013.

[39] "Renewables 2018." [Online]. Available: https://www.iea.org/renewables2018/.

[40] Y. Shen, J. L. Linville, M. Urgun-Demirtas, M. M. Mintz, and S. W. Snyder, "An overview of biogas production and utilization at full-scale wastewater treatment plants (WWTPs) in the United States: Challenges and opportunities towards energy-neutral WWTPs," *Renew. Sustain. Energy Rev.*, vol. 50, pp. 346–362, Oct. 2015.

[41] M. Yu *et al.*, "Combined Hydrogen, Heat and Power (CHHP) pilot plant design," *Int. J. Hydrogen Energy*, vol. 38, no. 12, pp. 4881–4888, 2013.

[42] T. A. Hamad *et al.*, "Hydrogen production and End-Uses from combined heat, hydrogen and power system by using local resources," *Renew. Energy*, vol. 71, pp. 381–386, 2014.

[43] T. A. Hamad *et al.*, "Study of a molten carbonate fuel cell combined heat, hydrogen and power system," *Energy*, vol. 75, no. 1, pp. 579–588, 2014.

[44] G. Rinaldi, D. McLarty, J. Brouwer, A. Lanzini, and M. Santarelli, "Study of CO2 recovery in a carbonate fuel cell tri-generation plant," *J. Power Sources*, vol. 284, pp. 16–26, 2015.

[45] P. Margalef, T. Brown, J. Brouwer, and S. Samuelsen, "Efficiency of poly-generating high temperature fuel cells," *J. Power Sources*, vol. 196, no. 4, pp. 2055–2060, 2011.

[46] Z. Lyu, H. Li, and M. Han, "Electrochemical properties and thermal neutral state of solid oxide fuel cells with direct internal reforming of methane," *Int. J. Hydrogen Energy*, vol. 44, no. 23, pp. 12151–12162, 2019.

[47] M. Pérez-Fortes *et al.*, "Design of a Pilot SOFC System for the Combined Production of Hydrogen and Electricity under Refueling Station Requirements," *Fuel Cells*, no. 0, p. fuce.201800200, 2019.

[48] D. McLarty, "UNIVERSITY OF CALIFORNIA , Thermodynamic Modeling and Dispatch of Distributed Energy Technologies including Fuel Cell – Gas Turbine Hybrids DISSERTATION submitted in partial satisfaction of the requirements for the degree of Doctor of Philosophy in Mechan," 2013.

[49] J. Brouwer, F. Jabbari, E. M. Leal, and T. Orr, "Analysis of a molten carbonate fuel cell: Numerical modeling and experimental validation," *J. Power Sources*, vol. 158, no. 1, pp. 213–224, Jul. 2006.

[50] G. Energy, *Modeling, Design, Construction, and Operation of Power*

*Generators with Solid Oxide Fuel Cells*. 2018.

[51] D. McLarty, J. Brouwer, and S. Samuelsen, "A spatially resolved physical model for transient system analysis of high temperature fuel cells," *Int. J. Hydrogen Energy*, vol. 38, no. 19, pp. 7935–7946, 2013.

[52] A. F. Massardo and F. Lubelli, "Internal reforming solid oxide fuel cell-gas turbine combined cycles (IRSOFC-GT): Part A- Cell model and cycle thermodynamic analysis," *J. Eng. Gas Turbines Power*, vol. 122, no. 1, pp. 27–35, 2000.

[53] D. Sánchez, R. Chacartegui, A. Muñoz, and T. Sánchez, "On the effect of methane internal reforming modelling in solid oxide fuel cells," *Int. J. Hydrogen Energy*, vol. 33, no. 7, pp. 1834–1844, 2008.

[54] E. Achenbach and E. Riensche, "Methane/steam reforming kinetics for solid oxide fuel cells," *J. Power Sources*, vol. 52, no. 2, pp. 283–288, 1994.

[55] E. Achenbach, "Three-dimensional and time-dependent simulation of a planar solid oxide fuel cell stack," *J. Power Sources*, vol. 49, no. 1–3, pp. 333–348, Apr. 1994.

[56] S. Campanari and P. Iora, "Comparison of finite volume SOFC models for the simulation of a planar cell geometry," *Fuel Cells*, vol. 5, no. 1, pp. 34–51, Feb. 2005.

[57] M. Ni, M. K. H. Leung, and D. Y. C. Leung, "Parametric study of solid oxide fuel cell performance," *Energy Convers. Manag.*, vol. 48, no. 5, pp. 1525–1535, 2007.

[58] D. Ferrero, A. Lanzini, M. Santarelli, and P. Leone, "A comparative assessment on hydrogen production from low- and high-temperature electrolysis," *Int. J. Hydrogen Energy*, vol. 38, no. 9, pp. 3523–3536, Mar. 2013.

[59] M. Fardadi, D. F. McLarty, and F. Jabbari, "Controlling spatial temperature variation in a rapid load following SOFC," *ASME 2013 11th Int. Conf. Fuel Cell Sci. Eng. Technol. Collocated with ASME 2013 Heat Transf. Summer Conf. ASME 2013 7th Int. Conf. Energy Sustain. FUELCELL 2013*, no. August 2015, 2013.

[60] M. Fardadi, D. F. McLarty, and F. Jabbari, "Investigation of thermal control for different SOFC flow geometries," *Appl. Energy*, vol. 178, pp. 43–55, Sep. 2016.

[61] M. Fardadi, F. Mueller, and F. Jabbari, "Feedback control of solid oxide fuel cell spatial temperature variation," *J. Power Sources*, vol. 195, no. 13,

pp. 4222–4233, 2010.

[62] M. MosayebNezhad, A. S. Mehr, M. Gandiglio, A. Lanzini, and M. Santarelli, "Techno-economic assessment of biogas-fed CHP hybrid systems in a real wastewater treatment plant," *Appl. Therm. Eng.*, vol. 129, pp. 1263–1280, 2018.

[63] E. M. Leal and J. Brouwer, "A thermodynamic analysis of electricity and hydrogen co-production using a solid oxide fuel cell," *J. Fuel Cell Sci. Technol.*, vol. 3, no. 2, pp. 137–143, 2006.

[64] M. Santarelli, F. Quesito, V. Novaresio, C. Guerra, A. Lanzini, and D. Beretta, "Direct reforming of biogas on Ni-based SOFC anodes: Modelling of heterogeneous reactions and validation with experiments," *J. Power Sources*, vol. 242, pp. 405–414, 2013.

[65] C. S. Montross, H. Yokokawa, and M. Dokiya, "Thermal stresses in planar solid oxide fuel cells due to thermal expansion differences," *Br. Ceram. Trans.*, vol. 101, no. 3, pp. 85–93, 2002.

[66] C. K. Lin, T. T. Chen, Y. P. Chyou, and L. K. Chiang, "Thermal stress analysis of a planar SOFC stack," *J. Power Sources*, vol. 164, no. 1, pp. 238–251, 2007.

[67] A. Selimovic, M. Kemm, T. Torisson, and M. Assadi, "Steady state and transient thermal stress analysis in planar solid oxide fuel cells," *J. Power Sources*, vol. 145, no. 2, pp. 463–469, 2005.

[68] F. Ranjbar, A. Chitsaz, S. M. S. Mahmoudi, S. Khalilarya, and M. A. Rosen, "Energy and exergy assessments of a novel trigeneration system based on a solid oxide fuel cell," *Energy Convers. Manag.*, vol. 87, pp. 318–327, Nov. 2014.

[69] A. Chitsaz, A. S. Mehr, and S. M. S. Mahmoudi, "Exergoeconomic analysis of a trigeneration system driven by a solid oxide fuel cell," *Energy Convers. Manag.*, vol. 106, pp. 921–931, 2015.

[70] J. F. Kast, "Dynamic Modeling, Design, and Performance Evaluation of Large Scale High Temperature Fuel Cell Tri-Generation Systems," *Mater. Sci. Eng. R Reports*, vol. 63, no. 3, pp. 100–125, 2009.

[71] P. Margalef, T. Brown, J. Brouwer, and S. Samuelsen, "Conceptual design and configuration performance analyses of polygenerating high temperature fuel cells," *Int. J. Hydrogen Energy*, vol. 36, no. 16, pp. 10044–10056, 2011.

[72] F. T. E. Station and F. Valley, "FUEL CELL TECHNOLOGIES OFFICE Tri-Generation Success Gas or Biogas."

[73] “DEMOSOFC project.” [Online]. Available: http://www.demosofc.eu/.

[74] P. I. DataBasi.org, “WWTPs on Southern California coast.” [Online]. Available: https://databasin.org/datasets/216db49227a24a8d8a3142524616657a.

[75] P. D. I. Torino, “L ’ uso del car sharing in Italia e un confronto internazionale,” 2018.

[76] Fondazione sviluppo sostenibile, “2° Rapporto nazionale sulla sharing mobility,” 2017.